Atwood, E. C., Falcieri, F. M., Piehl, S., Bochow, M., Matthies, M., Franke, J., Carniel, S., Sclavo, M., Laforsch, C., Siegert, F. (2019): Coastal accumulation of microplastic particles emitted from the Po River, Northern Italy: Comparing remote sensing and hydrodynamic modelling with in situ sample collections. - *Marine Pollution Bulletin*, *138*, pp. 561—574.

DOI: http://doi.org/10.1016/j.marpolbul.2018.11.045

Marine Pollution Bulletin 138 (2019) 561–574

Contents lists available at ScienceDirect

Marine Pollution Bulletin

journal homepage: www.elsevier.com/locate/marpolbul

Coastal accumulation of microplastic particles emitted from the Po River, Northern Italy: Comparing remote sensing and hydrodynamic modelling with *in situ* sample collections

Elizabeth C. Atwood[a,b,*], Francesco M. Falcieri[c], Sarah Piehl[d], Mathias Bochow[d,e], Michael Matthies[f], Jonas Franke[a], Sandro Carniel[c], Mauro Sclavo[c], Christian Laforsch[d], Florian Siegert[a,b]

[a] RSS Remote Sensing Solutions GmbH, Isarstr. 3, 82065 Baierbrunn, Germany
[b] Ludwig-Maximilians-Universität Munich, GeoBio-Center, Großhadernerstr. 2, 82152 Martinsried, Planegg, Germany
[c] Consiglio Nazionale delle Ricerche – Istituto di Scienze Marine (CNR-ISMAR), Arsenale-Tesa 104, Castello 2737/F, 30122 Venezia, Italy
[d] University Bayreuth, Dept. Animal Ecology I, Universitätsstr. 30, 95440 Bayreuth, Germany
[e] Helmholtz Centre Potsdam - GFZ German Research Centre for Geosciences, Telegrafenberg, 14473 Potsdam, Germany
[f] University of Osnabrück, Institute of Environmental Systems Research, Barbarastr. 12, 49069 Osnabrück, Germany

ARTICLE INFO

Keywords:
Beach sediment
River plume
FT-IR
ROMS
Landsat-8
Sentinel-2

ABSTRACT

Microplastic research has mainly concentrated on open seas, while riverine plumes remain largely unexplored despite their hypothesized importance as a microplastic source to coastal waters. This work aimed to model coastal accumulation of microplastic particles (1–5 mm) emitted by the Po River over 1.5 years. We posit that river-induced microplastic accumulation on adjacent coasts can be predicted using (1) hydrodynamic-based and (2) remote sensing-based modelling. Model accumulation maps were validated against sampling at nine beaches, with sediment microplastic concentrations up to 78 particles/kg (dry weight). Hydrodynamic modelling revealed that discharged particle amount is only semi-coupled to beaching rates, which are strongly mouth dependent and occur within the first ten days. Remote sensing modelling was found to better capture river mouth relative strength, and accumulation patterns were found consistent with hydrodynamic modelling. This methodology lays groundwork for developing an operational monitoring system to assess microplastic pollution emitted by a major river.

1. Introduction

Marine plastic litter has long been recognized as an environmental problem (Azzarello and van Vleet, 1987; Law and Thompson, 2014; Sheavly and Register, 2007) but only recently has begun to receive international attention at a level adequate to the potential severity of the threat (G7 Germany, 2015; GESAMP, 2016; UNEP, 2016). Microplastics, commonly defined as particles < 5 mm in diameter (Galgani et al., 2013), are increasingly proving to be ubiquitous in all water systems. Roughly 70 to 80% of marine debris comes primarily from land-based sources (Wagner et al., 2014), much being passively collected in waterways which eventually flow to the sea. Mani et al. (2015) found river water concentrations up to 3.9 million particles/km^2 in metropolitan areas along the Rhine River. Annual input of plastic particles to the Great Laurentian Lakes is estimated at 9.8 thousand tonnes (Hoffman and Hittinger, 2017). Despite the fact that freshwater systems are at least as severely contaminated as the oceans (Dris et al., 2015), large rivers have to date received relatively little attention (Mani et al., 2015; Wagner et al., 2014). An estimated 1.15 and 2.41 million tonnes enter the oceans each year from rivers alone (Lebreton et al., 2017), representing up to 50% of land based plastic emissions estimate, which ranges from 4.8 to 12.7 million tonnes (Jambeck et al., 2015). Once microplastics reach coastal waters, their dispersion and transportation pathways are governed by ocean and atmosphere dynamics; our understanding of these physical processes is still limited. Some authors suggest that how these processes influence microplastic transport may, to some extent, be comparable to well-studied suspended sediment transportation systems (Zhang, 2017), which could offer a more established framework for modelling suspended microplastic transportation.

* Corresponding author at: RSS Remote Sensing Solutions GmbH, Isarstr. 3, 82065 Baierbrunn, Germany.
E-mail address: atwood@rssgmbh.de (E.C. Atwood).

https://doi.org/10.1016/j.marpolbul.2018.11.045
Received 24 July 2018; Received in revised form 21 September 2018; Accepted 19 November 2018
Available online 08 January 2019

Microplastic transportation pathways are characterized by complex dynamics due to processes such as movement mechanisms (windage and sinking velocities) as well as changes in physical and chemical characteristics (loss of structural integrity, fragmentation and aggregation, see review Andrady, 2017) as well as interactions with biota (Law and Thompson, 2014). A combined hydrodynamic-Lagrangian transportation model effort would therefore be surely dependent upon necessary simplifying assumptions, as well as the quality of the hydrodynamic forcing data. Such models, with different degrees of realism, have been recently utilized to hindcast potential sources of stranded plastic litter in the Indian Ocean (Bouwman et al., 2016; Duhec et al., 2015), Aegean Sea (Politikos et al., 2017) and Adriatic Sea (Carlson et al., 2017). To date, little attention has been placed on local-scale river plume microplastic transport modelling in coastal seas (Browne et al., 2010; Carlson et al., 2017; Zhang, 2017). It is important to bear in mind that, due to the intrinsic model simplifications, dispersion pathways computed based on modelling results can accumulate errors over longer distances and times. Generally, modelling results should be considered qualitative rather than quantitative until validated against an independent dataset. A different type of model based on remote sensing acquisitions offers multiple depictions of the river plume that inherently include actual environmental conditions. While such an image displays the complex coastal ocean environment of the surface layer, it nevertheless offers restricted information for below the water surface and only represents the snapshot time period when the image was acquired.

In this paper, we implement and compare these two different types of models to assess how microplastics from a major river are spreading into a semi-enclosed sea and accumulate along its coastline. The objective is to create a coastal microplastic exposure map, which depicts accumulation of particles emitted from the Po River along the outer delta and covering southward the coastal area still under strong influence from the main Po River plume. Model (1) is a Lagrangian particle transportation model forced by a state-of-the-art hydrodynamic model, while model (2) is based on satellite remote sensing of river plume form and intensity along the coastline. We hypothesize that both models are able to capture coastal patterns in river plume emitted microplastic accumulation. Model results are validated against sediment sampling for microplastics from beaches with varying river plume exposure gradients. Development of a system to model coastal accumulation of microplastic debris from rivers would represent a very useful tool for agencies responsible for monitoring and reporting this pollution, as well as organization of clean-up activities and remediation strategies.

2. Materials and methods

2.1. Study area

The Adriatic Sea separates the Italian peninsula and Balkan coast, extending 800 km from the connection with the Ionian Sea over the Strait of Otranto northwest toward the Venice Lagoon (Fig. 1). The prevailing currents flow counterclockwise from the Strait of Otranto along the Balkan coastline and return southward with the Western Adriatic Current (WAC) along the Italian coastline (Artegiani et al., 1997a, 1997b; Carniel et al., 2016). The North Adriatic sub-basin is defined as the shallow area north of the 100 m isobath (Fig. 1).

The Po River provides the largest riverine influx to the Adriatic Sea, averaging daily 1500 m^3/s with streamflow ranging between 100 m^3/s and 11,550 m^3/s (Falcieri et al., 2014). Being the longest river in Italy, the Po River drainage area (74,000 km^2) encompasses much of the northern region of the country, with > 20 million inhabitants, and includes many large cities as well as areas of intensive industrial and agricultural activities (lower left inset Fig. 1). The river splits into many sub-rivers before flowing into the Adriatic Sea, the main recognized arms of which are the Po di Maistra, della Pila, delle Tolle, di Gnocca (or della Donzella) and di Goro (upper right inset Fig. 1). Additionally, there exist many side channels and lagoons, which also carry a portion of the river water to the sea. Notable among these side channels are the Busa di Scirocco and di Tramontana. The delta is an actively changing system with shifting sandbars that can obstruct outflow from a particular mouth (Simeoni and Corbau, 2009) and thus increase the outflow elsewhere. The highest river discharge occurs in the spring, associated with high precipitation and snow-melt runoff, and the lowest in autumn (Falcieri et al., 2014).

Both wind regime and freshwater influx play a deciding role in North Adriatic circulation patterns (Bignami et al., 2007; Bolaños et al., 2014; Falcieri et al., 2014). There are three main recognized wind regimes: Bora, Scirocco and Mistral. Bora events consist of strong, dry, northeasterly winds that tend to occur more often during the winter months, which together with low river discharge results in a small Po River plume that remains close to the coastline (Boldrin et al., 2009; Falcieri et al., 2014). As mentioned above, a Scirocco event comprises warm, humid, east-southeasterly winds that tend to occur more often during the spring to fall. This wind regime together with high river discharge results in a wider plume that can extend far across the Adriatic Basin. Mistral events are the least powerful of the wind regimes and are defined based on winds coming from the northwest, which have been found to minorly enhance WAC flow into the Ionian Sea (Bignami et al., 2007).

2.2. Sample design

The Po Delta field campaign was conducted from 4 to 25 June 2016, during which both water and sediment samples were taken. Water sample locations were selected to cover the main Po River, recognized river mouths and important subsidiary river mouths as well as the plume, ranging from near-coast waters to the plume outer edge (indicated by surface waters with salinity > 30 PSU). At each station, water samples used to estimate microplastic concentrations were collected from a small boat using a specially designed mini-manta trawl (300 μm mesh, further details available in S1 of the Supplementary material). A total of 24 water stations were sampled, the locations of which are indicated in Fig. 2 of the Results. The trawl net was rinsed before each sample collection by running the net without the cod end through the water for 5 min at the sampling location. One trawl pass per location was conducted alongside the boat for an average of 20 min and only when wind conditions were below Beaufort 2 (light breeze, 6–11 km/h). Samples were stored in glass jars until further processing in the lab. During trawling, *in situ* measurements were collected for sea surface temperature (°C) and salinity (PSU). Water clarity measurements (visibility depth with a Hydrobios secchi disk) were conducted both before and after each trawl. Additionally, 2 L water samples were concurrently collected from the water surface (top 40 cm) for later determination of the water parameters chlorophyll-*A* (Chl-*A*) and suspended particulate matter (SPM). Water samples were also processed for measurement of colored dissolved organic matter (CDOM, or Gelbstoff), but due to very low detected CDOM levels, these data were determined not useful for building a regionally calibrated remote sensing algorithm. Samples were kept dark while being stored in a cooler with ice until filtering later that the same day.

Chl-*A* samples were hand-pump filtered using Whatman GF/F glass microfiber filters (0.7 μm pore size), following the IOC and SCOR (1994) protocol. Filters were then wrapped in aluminum and stored at −20 °C for the duration of the field campaign, after which they were stored at −80 °C until further processing. Chl-*A* was extracted with 96% ethanol and analyzed with a JASCO FP-8600 fluorometer at an excitation wavelength of 435 nm and an emission wavelength of 670 nm. The fluorometer was calibrated using a photometer (JASCO V-670) and a Chl-*A* standard (C6144-1MG, Sigma-Aldrich). After the first measurements, samples were acidified with HCl and again measured to subtract phaeopigments from the chlorophylls to get concentration of Chl-*A* in mg/L following the JGOFS protocol (UNESCO, 1994).

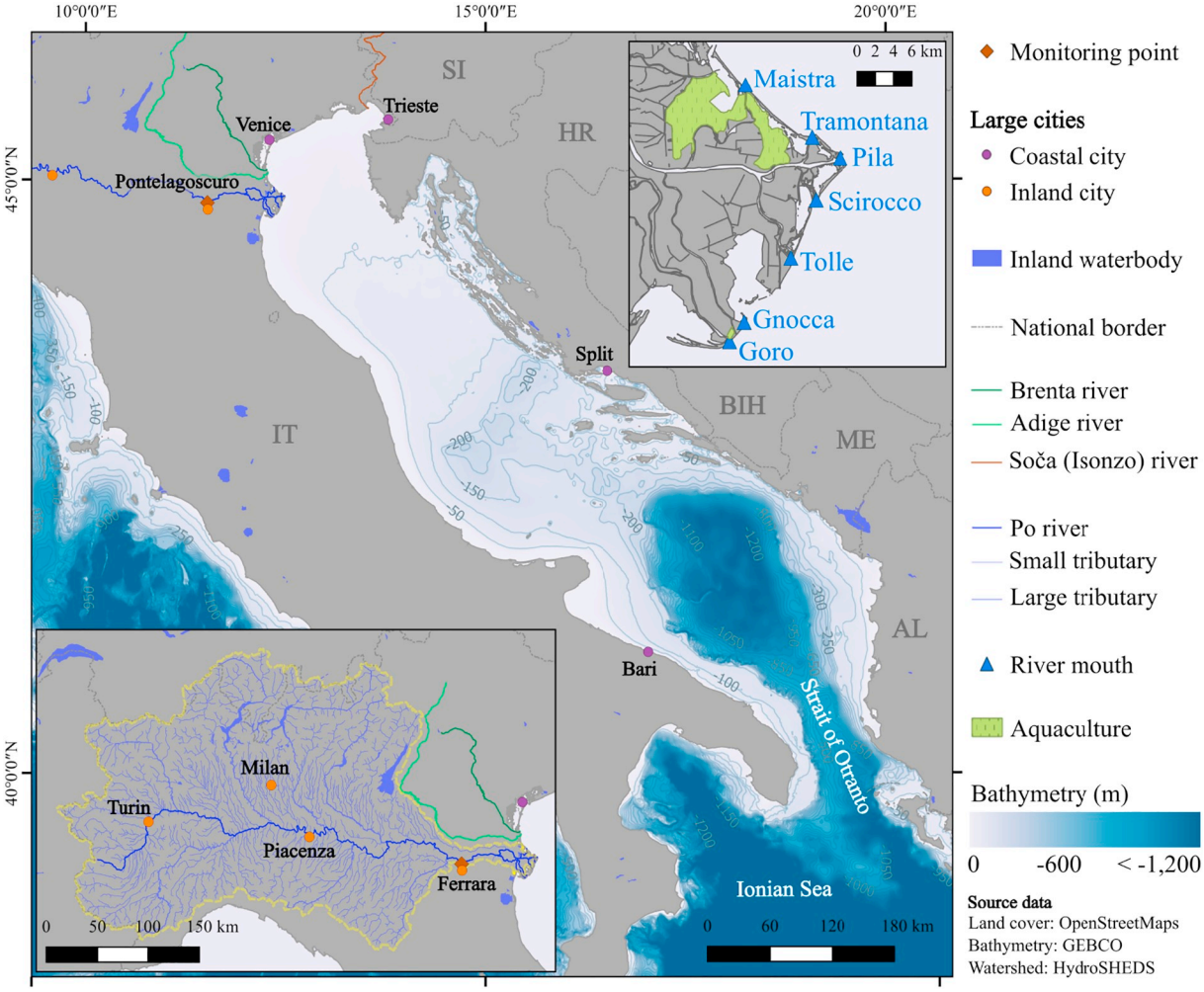

Fig. 1. Adriatic Sea overview map, showing bathymetry (contour lines follow 50 m depth intervals) along with large coastal cities and bordering countries: AL - Albania, ME - Montenegro, BIH - Bosnia and Herzegovina, HR - Croatia, SI - Slovenia, IT - Italy. Lower left inset shows Po River watershed (yellow dashed line) with large inland cities, as well as the Brenta (dark green line) and Adige (light green line) rivers. The Po Delta is displayed in the upper right inset, showing all five major river mouths (Maistra, Pila, Tolle, Gnocca and Goro) as well as important side channels (Tramontana and Scirocco) and dense aquaculture areas. (For interpretation of the references to color in this figure legend, the reader is referred to the web version of this article.)

SPM samples were hand-pump filtered using pre-weighed cellulose acetate filters with 0.45 µm pore size, air dried and stored in aluminum foil (Lindell et al., 1999). Filters were further dried in a 60–80 °C oven for 2 h and allowed to cool in a desiccator before weighting on a Sartorius R 200 D.

Surface reflectance measurements concurrent to each trawl were taken following the measurement methodology from Mobley (1999) and Fargion and Mueller (2000). An ASD FieldSpec 3 Hi-Res spectrometer was fitted with an 8° optic lens and set to measure raw digital numbers over an averaging of 50 rapid measurements. For each sampling location, a minimum of five measurement cycles were taken with the goal to collect as many cycles as possible during trawling. Each cycle consisted of a downwelling irradiance measurement over a white reference (nadir angle), an upwelling plus a sky radiance measurement both made following Mobley geometry (135° azimuth angle from sun, 40° off nadir for water and 40° off zenith for sky; Mobley, 1999), and lastly a repeated downwelling irradiance measurement to control for potential changes in lighting intensity conditions over the measurement cycle. All spectral measurement angles were estimated by hand and controlled by a second observer with a preset adjustable triangle. Measurement integration times were optimized for each measurement cycle in order to maximize signal. Downwelling irradiance was measured over a 90% Spectralon® white reference panel. Processing of raw digital numbers into remote sensing reflectance is discussed further in Section 2.5.

Sediment samples were collected from nine beaches in order to serve as a validation dataset for the hydrodynamic and remote sensing models (sample locations are indicated in the Results). Beach sample locations were selected so that three each of low, medium and high river plume impact areas would be represented. Estimates of river impact were based on the hydrodynamic modelling accumulation map (more details below in Section 2.4). At each location, samples were taken along the extreme high tide line, following protocols from Moreira et al. (2016) and Turra et al. (2014), and were only conducted between high tide cycles. The extreme tide line was defined visually as the area with the largest accumulation of drift material, which was found to always be a clearly separate line to the last high tide line. Samples were taken at equal intervals along a 100 m transect line, where the first 10 m were walked along the straight transect line and then turned at 90° for placement along the meandering drift line. Samples were taken with a 25 × 25 cm stainless steel quadrat and sampled to a depth of 5 cm. Wet weight of the samples were recorded and then sieved over 1 mm stainless steel mesh (matching model assumptions from the hydrodynamic model, more details below). Additionally, two 1 L bottles where filled with unsieved sand from the same transect line for later processing in the lab to convert the wet weight to dry weight.

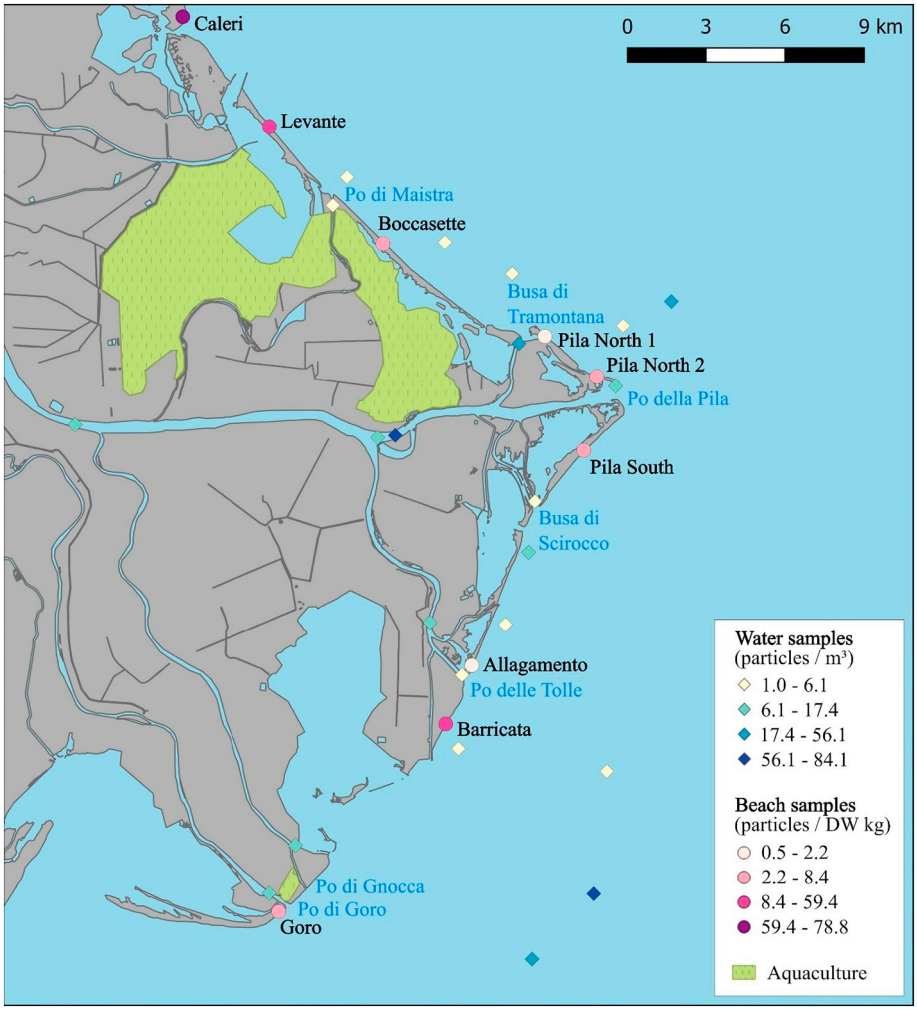

Fig. 2. Overview of water microplastic samples (diamonds, blue scale) and sediment microplastic samples (circles, pink scale) collected during the June 2016 field campaign. A total of 24 water locations and 9 beach locations were sampled, only beach locations are labeled (black text). Water samples are reported as particles/m^3 while sediment samples are reported as particles per dry weight kg (DW kg). River mouths are labeled in dark blue and dense aquaculture areas within lagoons are indicated. (For interpretation of the references to color in this figure legend, the reader is referred to the web version of this article.)

2.3. Microplastic sample processing

Water samples were first fractionated into two size classes: 5 mm–500 µm and 500–300 µm. To remove organic matter (which would disturb spectroscopic analysis) from the microplastic water samples, samples of the size class 500–300 µm were treated with enzymatic purification (Löder et al., 2017) and wet peroxide oxidation (Masura et al., 2015). For the latter class (size 5 mm–500 µm), samples with high organic content were treated solely with wet peroxide oxidation. All potential microplastic particles > 500 µm were visually presorted, photographed and stored for further analysis with Attenuated Total Reflectance (ATR) Fourier Transform Infrared (FT-IR) spectroscopy. For a full quantitative analysis of the fraction < 500 µm, samples were split. One subsample was filtered onto aluminum oxide membranes (Whatman Anodisc filters) and analyzed with Focal Plane Array (FPA) based Micro-FT-IR spectroscopy. The rest of the subsamples were filtered onto glass fiber filters (grade MN 85/90 BF) and analyzed with a newly developed shortwave infrared (SWIR) close-range imaging spectroscopy methodology called PlaMAPP (Schmidt et al., 2018) using a HySpex SWIR-320 m-e sensor (Norsk Elektro Optikk AS). This method allows counting microplastic particles, classifying the plastic type and determining particle size in a semi-automated way. Determination of plastic type is done by comparing the wavelength positions of the spectral absorption bands (local minima in the spectral signatures) of the recorded image spectra to those of plastic spectra from a reference spectral library.

Sediment samples along the 100 m transect were pooled, then processed by drying at 55 °C and separated from inorganic material using a zinc chloride solution (density 1.6–1.8 g/cm^3). The supernatant, which included both organic material and potential polymer particles, was collected using a self-made mote spoon (stainless steel, mesh size < 1 mm), rinsed with 98% ethanol and transferred into glass petri dishes. All potential microplastic particles were visually separated from organic material under a stereomicroscope (Leica M50 with cold light source Leica KL 300 LED, Leica Microsystems), photographed (attached Olympus DP26 camera, 5 Megapixel, Olympus Corp.) and identified to polymer type using ATR FT-IR spectroscopy.

Spectra of all potential microplastic particles > 500 µm, from both water and sediment samples, were recorded with a Tensor 27 FT-IR spectrometer (Bruker Optik GmbH) from 8 co-added scans within a spectral range from 4000 to 400 cm^{-1} and a spectral resolution of 8 cm^{-1}. Background scans were performed after every 10th measurement. Spectra were identified using the OPUS v7.5 software, correlating measured spectra against reference spectra from a custom in-house library (containing polymer spectra as well as spectra from both natural and lab materials used during sampling and processing, see Löder et al., 2015). Spectra of all potential microplastic particles < 500 µm were collected using the Tensor 27 FT-IR spectrometer further equipped with

a Hyperion 3000 FT-IR microscope that had a 15× cassegrain objective and a 64 × 64 FPA detector mounted. Spectra were obtained in transmission mode and measurement settings were as published by Löder and Gerdts (2015). Obtained chemical images were analyzed with the ImageLab v2.26 software and the BayreuthParticleFinder tool (developed during the project together with Epina Software Lab GmbH), which automatically highlights potential polymer particles on the chemical image obtained from the FT-IR measurements of the filter. Given that polymer spectra can diverge, dependent on factors such as particle size, thickness, color, polymer additives or adsorbed chemicals, all automatically detected particles were further manually controlled afterwards.

2.4. Hydrodynamic model

Simulations for microplastic dispersal from the Po River were performed from 1 January 2015 to 15 June 2016, to coincide with the field sampling campaign. A 3D Individual Based Lagrangian tracking model (ICHTHYOP; Lett et al., 2008) was implemented to simulate the dispersion of virtual microplastic particles (VMP) due to 3D currents and water column thermohaline structure. In the model, VMP behave as a Lagrangian drifter under the effect of horizontal/vertical advection and dispersion as well as buoyancy force due to the difference between the particle and surrounding water density. Particles were assigned a spherical shape (diameter of 1 mm) and density of 0.91 g/mL. Density was chosen to correspond with the averaged density of virgin polyethylene (both high and low density) and polypropylene, which together account for over 48% of EU demand (PlasticsEurope, 2014) and represent the majority of sampled microplastic debris (Imhof et al., 2013; Zbyszewski and Corcoran, 2011). Horizontal dispersion was included with a turbulent dissipation rate of $\epsilon = 10^{-7}\ m^2/s^3$, in agreement with turbulent kinetic energy observations in the Adriatic Sea. VMP were tracked for a total of 60 days, in excess of Adriatic particle half-life model estimates (Liubartseva et al., 2016) and drifter mean half-life observations (Poulain, 2001) of *circa* 40 days.

Simulations were based on the simplifying assumption of a constant concentration of 10 microplastic particles/m^3 in river waters, as reported in previous observations from the Po River (van der Wal et al., 2015; Vianello et al., 2015). Given that the river is represented as a point source inside the hydrodynamical model, VMP were released at the surface along straight 500 m transects located 250 m in front of each river mouth, with the goal being to mimic a direct discharge from the river itself. Po River mouths included Maistra, Pila, Tolle, Gnocca and Goro plus the Busa di Scirocco (given its presence in the hydrodynamic model). VMP were released over the entire simulation period at hourly intervals from all six locations, and the total number of VMP released at each mouth was determined based on the water discharge distribution among the main branches of the Po River.

Once released, a VMP was considered beached if it passed closer than 250 m from the coastline. This fixed distance was set based on the model spatial resolution (half the horizontal grid size) and in consideration that the model has difficulty representing complex nearshore processes. VMP were tagged with release date and river mouth, so that relative contribution from each river mouth could later be assessed. Once identified as beached, the VMP was removed from the dataset. VMP resuspension after beaching was not accounted for in the model, given the still existing amount of uncertainty surrounding this process (Hardesty et al., 2017; Zhang et al., 2017). This approach could lead to a small overestimation of beaching rates, but it was decided that a simplifying approach was preferable to setting an arbitrary factor meant to represent resuspension and similar nearshore processes.

ICHTHYOP simulations were run offline using as physical forcing an elaboration of the UNIVPM-Regione Marche operational hydrodynamic model that covers the northern Adriatic Sea (horizontal resolution of 500 m; 12 vertical sigma layers). The model (ROMS, Regional Ocean Modelling System; Haidvogel et al., 2008; http://myroms.org) was implemented in a coupled version with a surface wave model (SWAN, Simulating WAves Nearshore model; Booij et al., 1999; http://swan.tudelft.nl) through the COAWST (Coupled-Ocean-Atmosphere-Wave-Sediment Transport Modelling System; Warner et al., 2010; Warner et al., 2008). Surface forcings were derived from COSMO-I7, a local implementation of the Lokal Model (Steppeler et al., 2003) developed in the framework of the COSMO Consortium (http://cosmo-model.org) and run by the Agenzia Regionale per la Prevenzione, l'Ambiente e l'Energia dell'Emilia Romagna - Servizio Idro-Meteo-Clima (ARPA ER-SIMC). The UNIVPM-Regione Marche model implementation was chosen because it was the only freely available and operationally running forecast model with a high horizontal resolution for the Adriatic Sea.

A coastal reference grid was developed for displaying the distribution of beached particles along the Po Delta shore. To avoid artificial "shadowing" effects from corners of the hydrodynamic model grid cells located along the coastline, a smoothed grid was established based rather on the coastline. This grid was created with ArcGIS v9.31 software by projecting the coastline 250 m offshore, separating this into 500 m segments and buffering each segment with 250 m, producing grid cells variable in both shape and surface but without sharp angles or abrupt changes in direction. After post processing, distribution maps of estimated accumulation could be defined for each day up to the entire simulation period. Beach sediment sampling transect locations were placed as close as possible to the middle of the modelled accumulation pixel.

2.5. Near-range spectral measurements and remote sensing model

The remote sensing model for quantifying coastal exposure to riverine-based microplastic particles was based on the assumption that suspended microplastic particles are transported by the same mechanisms as other passive, suspended water constituents for which well-established remote sensing methodologies exist. With the goal being to optimally capture river plume water reflectance characteristics, near-range spectral measurements were used to build regionally calibrated remote sensing spectral reflectance water parameter algorithms for different satellite platforms.

First, raw digital number measurements from the spectroradiometer of downwelling irradiance plus upwelling and sky radiance were converted to irradiance, E(z, λ) in units of W/(m^2 nm), and radiance, L (z,θ,φ,λ) in units of W/(m^2 sr nm), using the software package RS^3 version 6.4.0 from ASD Inc. Radiance measurements were visually checked for abnormal behavior (such as saturation or detector jumps) before being converted to remote sensing reflectance (R_{RS}) following the methodology described by Heim (2005):

$$R_{RS}(0+,\lambda) = \frac{L_{total}(0+,\lambda) - r_{wa}xL_{sky}(\lambda)}{E_{down}(0+,\lambda)}\ [sr^{-1}]$$

where $R_{RS}(0+,\lambda)$ is the remote sensing reflectance directly above the water surface (0+) for a given wavelength (λ), L_{total} is the above water (upwelling) radiance measurement, r_{wa} is the proportion of directly back-reflected skylight at the air-water interface (taken here to be 0.021, following Heim, 2005), L_{sky} the sky radiance, and E_{down} the downwelling irradiance measurement.

The ASD R_{RS} dataset from the field campaign together with the *in situ* SPM measurements were used to calibrate various candidate algorithms to the Po River region and for a given satellite sensor, the best of which was then selected as the optimal regionally calibrated empirical algorithm for the time series analysis. Four separate algorithms for spectral detection of SPM were considered: (i) Jørgensen (1999) based on the CZCS band 3 detecting in the range 540–560 nm, (ii) Dekker (1993) based on *in situ* spectrometer measurements at 706 nm, and two different SPOT-3 ratio-based algorithms from Doxaran et al. (2002) based on (iii) band 3 (780–890 nm) divided by band 1 (500–590 nm)

and (iv) band 3 divided by band 2 (610–680 nm). All calibrated models were assessed for quality *via* Root Mean Square Error (RMSE) as well as goodness of fit statistics following the methods of the Ocean Color Group (Campbell and O'Reilly, 2005). This allowed determination of the best-calibrated SPM algorithm for Po River water with a particular satellite. Both the "Baseline" and "Calibrated" fits were also assessed for data overfitting using a leave-one-out cross-validation (LOOCV) technique (Michaelsen, 1987). Further details regarding the calibration and validation process are available in S2 of the Supplementary material.

Landsat 8 (L8), a joint mission of the U.S. Geological Survey (USGS) and National Aeronautics and Space Administration (NASA), is equipped with two push-broom sensors, the Operational Land Imager (OLI) and the Thermal Infrared Sensor (TIRS), which provide multispectral images with 30 m spatial resolution. The Po Delta study area is located in the overlap region between two Landsat flight paths, thus reducing the revisit time for this particular study to 7 days. The European Space Agency (ESA) Sentinel-2 (S-2) mission is a constellation of two identical satellites that are equipped with a push-broom MultiSpectral Instrument (MSI) sensor. S-2 provides multispectral images with 10, 20 and 60 m spatial resolution depending on the spectral band. S-2 has a revisit time of up to 2–3 days at midlatitudes. Usable images from L8 and S-2 acquired between 1 January 2015 and 30 June 2016 were compiled. Other platforms with coarser image spatial resolution (≥300 m) but proving daily (MODIS) to 2-day (Sentinel-3) acquisitions with much greater Signal-to-Noise Ratio (SNR) were considered but not implemented given that our goal was to capture the fine river plume structure as close to the coastline as possible.

Different atmospheric correction algorithms were tested to minimize the introduction of artifacts to the bands needed for detection of various water parameters, which was accomplished through comparison with concurrent *in situ* R_{RS} spectrometer measurements (further details in S3 and S4 of the Supplementary material).

The L8 and S-2 acquisitions were processed with a hierarchical object-based image analysis (OBIA) developed with eCognition software (Trimble Navigation Ltd.) to remove land, cloud, boats, white caps and breaking waves. The masked images were then used to create SPM concentration maps, which showed how the river plume was spreading into the surface coastal waters over the examined time period.

For each acquisition date, non-coastline pixels were masked and the remaining utilized as the basis for creating the coastline riverine microplastic exposure map. This was accomplished by converting pixel values to a similarity ratio using the average SPM concentration from all five river mouths for that acquisition date. The goal was to display how similar a given coastline pixel was to a pure river water pixel, which was then used to indicate influence from river plume waters along the coastline. Data were binned into hexagons to allow for combination of images with differing footprints as well as spatial resolution, at diameters of both 30 m and 100 m. This was accomplished using the "hexbin" package within the R software package (R Core Team, 2016). The first diameter represents the minimum allowable resolution and the second to match the sediment sampling scheme as well as easier visualization of the entire Po Delta coastline. Gaps in the dataset, produced through masking areas such as cloud cover or breaking waves, were filled in the time series using a combination of Nearest Neighbor Filtering and temporal linear interpolation. This was done again in R using the packages "raster", "rgdal", "rgeos", "sp" and "spacetime". SPM values between L8 and S-2 images were compared using standardized differences to check for any inherent bias between the different sensors. The time series was then summed to create a composite image of river plume influence along the Po Delta coastline for the entire modelled time period.

Po River gauge measurements were obtained for the modelling period from ARPA ER, taken at Pontelagoscuro. Wind regime in front of the Po Delta was estimated by extracting the zonal and meridional wind components from the COSMO I7 dataset (forcing field used in the hydrodynamic model) for eight points located 20 km in front of the coastline. For each point, the daily average magnitude and heading were first computed, and then all eight points averaged to obtain a single value representative of the whole area. Significant wind regime events were identified as days with an average wind speed over 5 m/s and consistently blowing from northeast (Bora), southeast (Scirocco) or northwest (Mistral).

2.6. Validation of the modelled microplastic exposure maps

Modelled microplastic accumulation values from both the remote sensing time series as well as the hydrodynamic particle tracking were compared to *in situ* beach sediment microplastic concentrations to assess model validity as well as identify weaknesses and strengths of each modelling method. Comparisons were made using both Pearson's Correlation r as well as Spearman's Rank Coefficient ρ. All calculations were carried out using R software. Model maps were also compared to one another by unit-base normalizing (also known as feature scaling) each map and then comparing difference values at regular latitudinal intervals along the coastline.

3. Results and discussion

3.1. Water parameter sampling

Water parameter field measurements are presented in Table 1. Chl-*A* measurements fell within 0.005–0.043 mg/L, and SPM values covered a moderate range as compared with ARPA ER monitoring measurements of SPM from Pontelagoscuro (for the time period January 2015 to June 2016, these ranged from 12 to 372 mg/L). Secchi depth measurements only reached a maximum of 163 cm, all located along the outer edge of the river plume.

3.2. Microplastic sampling

Water microplastic samples analyzed by ATR FT-IR and SWIR spectroscopy ranged from 1 to 84 particles/m^3 (Fig. 2), with the highest concentrations being found along the outer river plume edge, within the main arm of the river (Po della Pila) and the side channel Busa di Tramontana. The Maistra and central Tolle river mouths both had very low concentrations, < 6 particles/m^3. Repeated measures from a particular river section, such as where Po delle Tolle separates from Pila or where Tolle splits into three channels before entering the Adriatic, indicated large variability from one sampling time to another.

Some of the highest *in situ* water microplastic measurements were found along the outer edge of the Po River plume, which suggests that either microplastic concentrations in the open Adriatic are at least comparable with those from the river, or that there are local accumulation processes occurring along the front between fresh river water and much higher salinity ocean water. Given that rivers are considered one of the main sources of plastic debris to the ocean (Jambeck et al., 2015; Lebreton et al., 2017) together with evidence that the Adriatic Sea is a highly dissipative system (Horvat, 2015), the latter hypothesis is more likely. Furthermore, concentrations found in this study are an order of magnitude higher than values measured by Suaria et al. (2016) in the open Adriatic Sea. Using the median *in situ* measured microplastic

Table 1
Measured water parameters during the field campaign. Chlorophyll-*A* (Chl-*A*) and suspended particulate matter (SPM) reported in mg/L, Secchi depth average from before and after trawl in cm.

	Chl-*A* (mg/L)	SPM (mg/L)	Secchi (cm)
Mean/Median	0.011/0.009	30.2/21.1	67/51
Standard deviation	0.008	29.4	36
Maximum	0.043	127.9	163
Minimum	0.005	7.7	29

Table 2
Sediment microplastic overview for all 9 beaches sampled, listed north to south. Percent contribution from each plastic type identified is listed: PE polyethylene, PP polypropylene, PS polystyrene ([1] also includes ABS acrylonitrile butadiene styrene and SAN styrene acrylonitrile), PA polyamide, EV accounts for EVOH ethylene vinyl alcohol and EVA ethylene vinyl acetate, PEST polyester, PET polyethylene terephthalate, PVC polyvinyl chloride, PUR polyurethane, PVAL polyvinyl alcohol, SBR styrene butadiene rubber, C/U accounts for either composite particles or unknown plastic types. Total microplastic particles found as well as particles/DW kg is indicated for each beach sampled.

Beach	% contribution												Tot. part.	Part./DW kg
	PE	PP	PS[1]	PA	EV	PEST	PET	PVC	PUR	PVAL	SBR	C/U		
Caleri	45.0	8.6	28.0	< 1	18.0	< 1	< 1	< 1	< 1	0	0	< 1	3080	78.8
Levante	62.2	14.6	16.4	< 1	5.7	< 1	< 1	< 1	< 1	< 1	< 1	< 1	2032	59.4
Boccasette	42.9	13.2	42.9	0	< 1	0	0	0	0	0	0	< 1	182	3.9
Pila North 1	27.0	14.8	54.8	0	< 1	0	< 1	0	0	0	0	< 1	115	2.2
Pila North 2	60.2	9.7	20.4	1.9	0	< 1	4.9	0	< 1	0	0	< 1	103	3.6
Pila South	45.7	18.9	34.1	0	1.4	0	0	0	0	0	0	0	440	8.4
Allagamento	10.0	5.0	85.0	0	0	0	0	0	0	0	0	0	20	0.5
Barricata	19.2	13.8	66.3	< 1	< 1	0	0	0	0	0	0	0	652	14.3
Goro	52.0	19.0	27.8	0	< 1	0	0	0	0	0	0	< 1	248	5.2

concentration from this study together with average Po River discharge (1500 m^3/s) and estimates of microplastic particle count to weight in the Adriatic (1.68 to 3.00 mg/particle; Suaria et al., 2016; van der Wal et al., 2015; Vianello et al., 2015), a rough estimate of floating microplastic released by the Po River ranges between 2.2 and 3.8 t per day. This translates to between 785 and 1402 t/yr, coming close to the estimates of 1349 t/yr by Liubartseva et al. (2016), although it should be noted the latter estimate is based on vertical water column integrated estimates of all plastic debris (both macro and microplastics). Our estimate should be taken with care given that the microplastic sampling method utilized in this study only sampled microplastics floating at the water surface, which has been shown to often underestimate total floating microplastic concentrations (Brunner et al., 2015; Kooi et al., 2016).

The beach sediment microplastic samples (Fig. 2) ranged from 0 to 78 particles per dry weight (DW) kg. The highest measurement by far was on the northernmost beach, Caleri, where a total of 3080 microplastic particles were identified for the entire transect (Table 2). Polystyrene (PS), acrylonitrile butadiene styrene (ABS) and styrene acrylonitrile (SAN) were found to have similar spectral signatures, thus were pooled into a group called styrene-based polymers to avoid potential confusion between these types. The same was true for the polymer types ethylene vinyl alcohol (EVOH) and ethylene vinyl acetate (EVA). Polyethylene (PE), polypropylene (PP) and the styrene polymer group made up > 97% of all particles sampled on six beaches (Boccasette, Pila North 1, Pila South, Allagamento, Barricata and Goro). Beach sediment particles identified as belonging to the styrene polymer group were most often found in their foamed form, which is not surprising considering that the non-foamed polystyrene is less dense than seawater. The remaining three beaches had either an increased contribution from EVOH/EVA or, in the case of Pila North 2, elevated contributions for the polymer types polyamide (PA) and polyethylene terephthalate (PET).

The top three contributing polymer types from the beach sediment microplastic concentrations were PE, styrene-based polymers and PP, in step with general trends observed in both the Po River (van der Wal et al., 2015) and the Mediterranean Sea (Suaria et al., 2016) as well as coastal (Zhang, 2017) and global oceans (Andrady, 2017). PE and PP make up between 45 and 50% of total global plastic production (PlasticsEurope, 2016). Higher occurrence of other plastic types, especially the heavier polymers such as EVOH, PVAL, PET (polyethylene terephthalate) and PVC (polyvinylchloride), were found at Caleri, Levante and Pila North 2 (Fig. 2 and Table 2). Caleri in particular was found to have the most extreme microplastic concentration, exceeding the measurement by Munari et al. (2017) of 21 particles/DW kg at Volano, just south of the Po Delta. It is important to note that a possible explanation for this could be different sampling locations, as this study sampled the extreme high tide line in contrast to the most recent high tide line. Our measurements were lower than those made in the Venice Lagoon (672–2175 particles/DW kg; Vianello et al., 2013), although it should be noted that smaller size classes were under investigation in the study by Vianello et al. and it is often the case that particle abundances increase with decreasing size class (Imhof et al., 2018; Lee et al., 2013). The two northernmost beaches surveyed in this study (Caleri and Levante) were located close to either a public parking lot or a harbor. Heavier particles are known to be transported more slowly than particles which are less dense than surrounding seawater (Cable et al., 2017), which include the plastic types EVOH, PVAL, PET and PVC in their virgin form. This suggests that the higher concentration rates more likely result from local sources, rather than longer distance transportation by the Po River plume or other Adriatic currents.

3.3. Time series data and hydrodynamic model accumulation

River discharge and wind speed, overlain with wind regimes, are shown in Fig. 3 together with total daily beached VMP and a pictorial overview of satellite acquisition coverage (discussed in more detail in the following Section 3.4). The highest observed daily wind speeds (Fig. 3a) occurred in February, March and November 2015, and March 2016, which all corresponded to northeast winds (Bora events, light blue bars in Fig. 3). Scirocco events (southeast wind, green bars) were observed to have less strong wind speeds. Both Mistral and Scirocco events were found to have occurred less frequently than Bora events.

Comparing Po River average daily outflow with the total daily beached VMP (Fig. 3b), a loose connection between streamflow and number of beached VMP was evident. This comes as no great surprised since Po River streamflow was inherently linked to daily particle release rate in the model. High beaching rates in February, June and October 2015 were observed to follow high river discharge events, but this pattern was not always present. Beaching peaks in July 2015 and January 2016 did not correlate with high river discharge events, hinting that beaching is not only driven by the amount of released VMP but also by the surface current field close to the coast and winds.

Of all VMP released, only 18% were found to beach during the simulations. The ratio of released-to-beached VMP for each mouth was highly variable. Po della Pila, Busa di Scirocco and Po di Gnocca river mouths were found to beach < 10% of all VMP released, while Po di Maistra and delle Tolle presented higher rates (26% and 19% respectively). By far the highest rate of beaching was determined for the southernmost river mouth, Po di Goro, with 94% of all released VMP being found to have beached. In Fig. 4a, the percentage of beached VMP from a particular river mouth are compared with the total VMP beached for each model run day. The other river mouths (Maistra, Pila, Scirocco, Tolle and Gnocca) display similar behavior in that the majority of

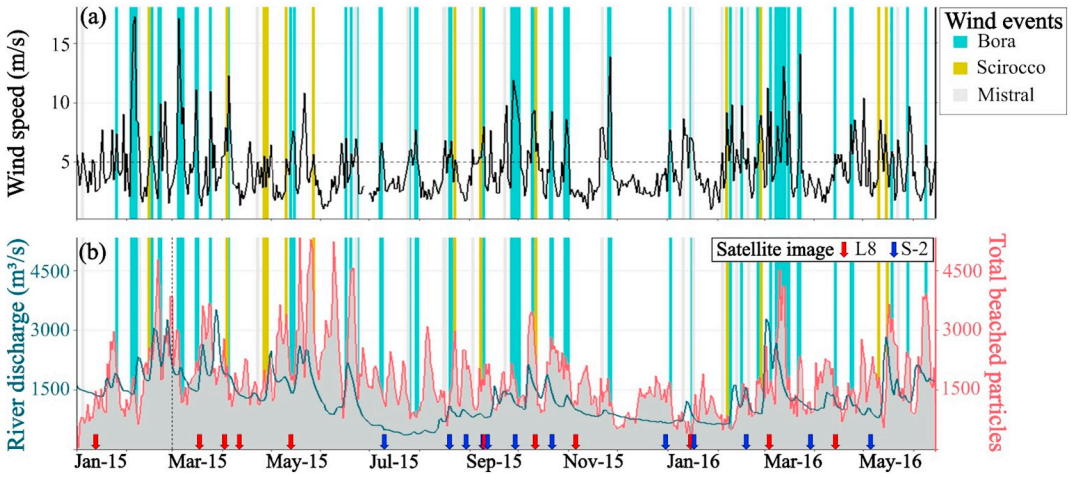

Fig. 3. (a) Average daily wind speed (m/s) in front of the Po Delta. Colored bars highlight wind events: Bora (light blue), Scirocco (green) and Mistral (light gray). Horizontal dashed line depicts the 5 m/s wind speed threshold. (b) Average daily Po River outflow (m^3/s) at Pontelagoscuro (dark blue line, left axis) compared with the average daily total of beached virtual microplastic particles (VMP, rose line, right axis). VMP were tracked in the model a total of 60 days, with the first day that satisfied this condition indicated by the vertical dashed black line. Usable satellite acquisitions are depicted by arrows (Landsat 8: L8, red; Sentinel-2: S-2, blue) along the temporal horizontal axis, ticked below to separate months. Wind events displayed as in (a). (For interpretation of the references to color in this figure legend, the reader is referred to the web version of this article.)

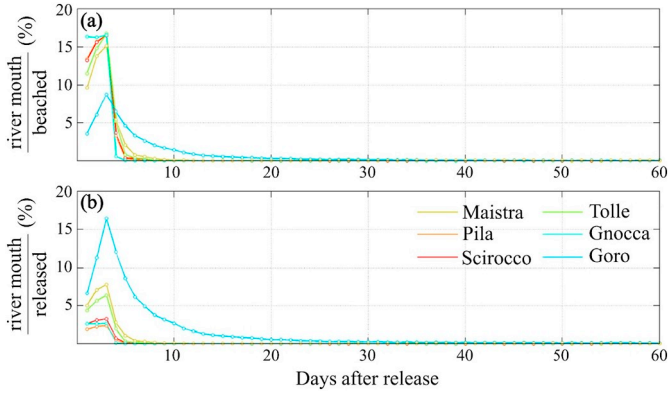

Fig. 4. Percent beached virtual microplastic particles (VMP) from each river mouth in comparison to (a) total daily beached VMP and (b) total daily released VMP. Days after release are depicted along the horizontal axis. Release events after April 15th, 2016, are not included since these were run for < 60 days.

beaching occurs within the first 3 days and was then followed by a sudden drop to low values, remaining close to zero after about 10 days. The Po di Goro mouth, on the other hand, also displayed high beaching rates in the first 5 days but thereafter a more gradual decline, reaching zero levels after *circa* 20 days. Thus, VMP released by the Po di Goro mouth were able to reach the coastline for a longer period of time (up to 30 days after release, as shown in Fig. 4a) and thus had higher probability to be beached than VMP released from the other mouths. Fig. 4b depicts the percentage of beached VMP per river mouth as compared to the total VMP released by the same river mouth. Here the much larger percentage of VMP to become beached from the total released by the Po di Goro mouth was quite clear, with over 34% of all VMP released from the river mouth being beached within the first three days after release. The elevated beaching rates of the Po di Maistra and delle Tolle were also more clearly depicted.

The hydrodynamic model beaching accumulation map for the entire simulation period is shown in Fig. 5. VMP release points in front of river mouths are indicated by the red arrows. Higher beached VMP accumulation was evident locally around each of the river mouth release points (Fig. 5a), as well as along the southern coast of the Po Delta and extending along the southward coast. The highest accumulation areas were modelled to be just south of the Po della Pila river mouth, and near to the Po di Gnocca and di Goro river mouths. The individual distribution from each river mouth is depicted in Fig. 5b, showing that the VMP beaching rates for all mouths remain quite local except for the southernmost Po di Goro mouth.

The hydrodynamic modelling results suggest that surface currents play a more deciding role in determining beaching rates, with the number of particles being released by the river only semi-coupled to beach accumulation. Surface currents in the northern Adriatic are determined by wind regime and freshwater influx, the Po River being the main contributor (Falcieri et al., 2014). VMP tracks from different river mouths revealed beaching rates of up to 18% for all modelled river mouths, with the exception of the southernmost mouth Po di Goro. This is a result of the Goro freshwater plume likely being held closer to the shoreline by the other plumes, thus allowing plume water to interact with the coastline for a longer period of time. For the other river mouths, VMP beaching was found to occur within 10 days following release, and beaching rate estimates suggests that over 80% of the microplastic particles being released by the Po River are being dispersed to the open Adriatic Sea system.

3.4. Remote sensing model accumulation

Results of all four assessed SPM algorithms are presented in Table 3, where the algorithm basis is listed along with the fitted algorithm and model fit statistics (RMSE, LOOCV-RMSE, bias). Model fit statistics were found to be reduced by an order of magnitude through the calibration/validation for both the Jørgensen and Dekker algorithms, only slight improvement was achieved for one of the band-ratio Doxaran algorithms while the other was found to be a non-significant predictor for the Po River water. Given the observed overlap of the Chl-*A* reflectance peak at 560 nm with the SPM signal saturation between 550 and 700 nm, the Dekker algorithm was selected as preferable to the Jørgensen algorithm (further details in S5 and S6 of the Supplementary material). Furthermore, the Dekker algorithm was found to be a significant predictor for both L8 as well as S-2 data.

A total of 26 usable images from L8 and S-2 (12 and 14 respectively) were compiled covering the modelling time period (as shown in Fig. 3 and Table 4). Usable images from two out of the total eighteen months considered could not be obtained. Of the compiled usable satellite images, five instances of Bora/low discharge were captured, as well as three instances of Scirocco/high discharge, only two instances of Bora/

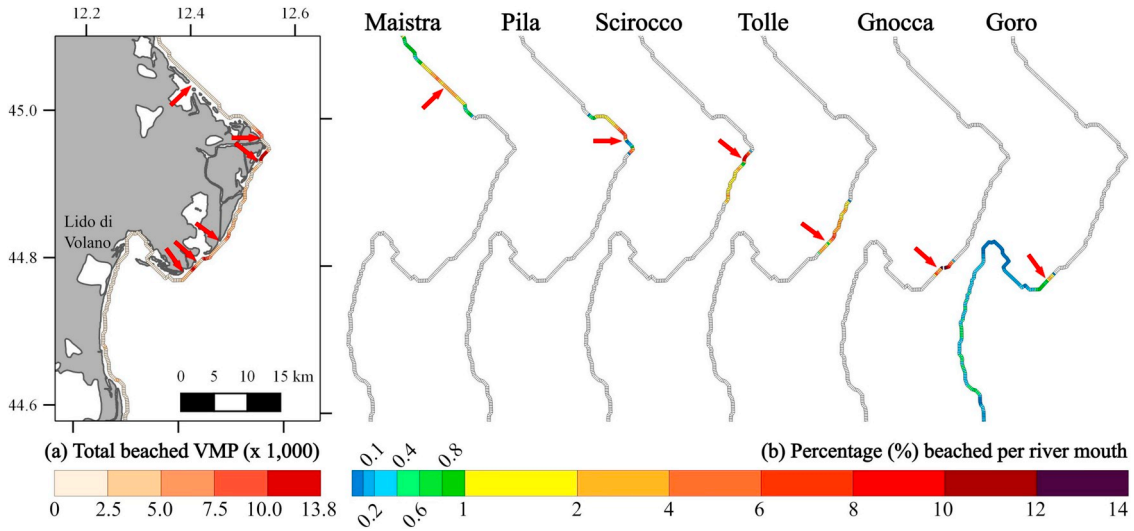

Fig. 5. (a) Distribution map for virtual microplastic particle (VMP) beaching accumulation over the entire 1.5-year simulation period, VMP release locations in front of river mouths are indicated by the red arrows. Color scale (beige low, red high) indicates total particles beached over entire modelling period. (b) Beached VMP for each river mouth displayed separately, color scale (blue low, red high) indicates percentage of total VMP beached from that particular river mouth. (For interpretation of the references to color in this figure legend, the reader is referred to the web version of this article.)

high and Mistral/high, and one instance each of Scirocco/low and Mistral/low discharge conditions. Images were atmospherically corrected (further details in S3 and S4 of the Supplementary material) and the optimal calibrated regional empirical algorithm for each sensor was implemented to create a time series of SPM river plume maps.

Examples from satellite image masking and implementation of the calibrated SPM algorithm are shown in Fig. 6. High/low river discharge was classified as daily average river discharge over/below the median discharge rate for the entire modelling period (1210 m^3/s). From the acquisition with high discharge, the strong effect of a wind event on river water transportation was quite evident. In the case of high discharge together with southeasterly Scirocco winds (Fig. 6b), plume water can be observed being pushed northward of the Po della Pila mouth. With northwesterly Mistral winds (Fig. 6c), the plume shape appears to be more heavily influenced by river outflow, with high river discharge producing a plume extending further into the Adriatic. But in the case of northeasterly Bora winds (Fig. 6a), the high discharge plume was kept closer to the coastline while primarily spreading high SPM waters toward the south. A somewhat different pattern was observed for the acquisitions concurrent to low discharge. The Bora wind event on January 16, 2016, was observed to again retain the plume close to the southern coastline (Fig. 6d). Plume form under low discharge and Scirocco wind was only demonstrated with one acquisition (Fig. 6e). SPM signal from the river water on this date were quite low, making the plume difficult to detect, but through utilizing a different stretch the plume could be observed to extend further into the Adriatic. The Mistral wind together with low discharge (Fig. 6f) was observed to retain the river plume close to the coastline, but much smaller than was observed with high discharge. Standard difference comparison between L8 and S-2 images revealed a slight sensor bias, in that detected L8 SPM values tended to be less (< 2 mg/L) than detected S-2 SPM values. This amount represented < 2% of the SPM range measured in the field (Table 1) and was thus taken to be negligible.

Results of the remote sensing composite hexagon binning processing are presented in Fig. 7, with red indicating coastal areas of high river water influence and green areas with less. Strong river water influence was detected around all five river mouths (Maistra, Pila, northern and central Tolle, Gnocca and Goro) as well as the Busa di Tramontana and di Scirocco. The southern arm of the Po delle Tolle was observed to have a lesser influence, while the northern section of coastline between river mouths presented very low rates of river water influence. Coastline sections near to the Po della Pila mouth and southward were observed to have higher rates, with the highest influence evidently being along the coastal section just north of Po della Pila. An area of very high river water influence (red) was detected between Po della Pila and Busa di Tramontana, which corresponds to an additional river mouth flowing out from the lagoon that was first observed during the field campaign.

Coastal exposure modelling using SPM derived from remote sensing images was able to well capture the signal of sediment heavy river plume waters spreading along the coastline (Fig. 6 and Fig. 7). Plume

Table 3
Calibrated algorithms for suspended particulate matter (SPM). Algorithm spectral basis and publication is indicated in the first column, standard fit algorithm in the second column together with model fit statistics: root mean square error (RMSE) and bias. Baseline and satellite specific algorithms are listed in the following columns, with fitted algorithm listed followed by fit statistics (RMSE, leave-one-out cross-validation RMSE, bias) in parentheses. Relationships that were found to be non-significant ($\alpha \geq 0.05$) during fitting are indicated with N/A. The satellite sensor band used is also indicated, *e.g.* Landsat 8 band 3 centered at 560 nm is indicated by $b3_{560}$.

Algorithm basis	Standard fit	Baseline fit	Landsat 8	Sentinel-2
Band at 555 nm (Jørgensen, 1999)	$0.09 + 56.19 * b_{555}$ (154.91; 148.22)	$\exp(1.47 + 0.60 * b_{555})$ (40.66; 29.98; 27.67)	$\exp(1.46 + 0.60 * b3_{560})$ (40.64; 29.35; 27.67)	$\exp(1.45 + 0.60 * b3_{561})$ (40.65; 29.63; 27.67)
Band at 706 nm (Dekker, 1993)	$2.69 + 3.31 * b_{706}$ (561.16; 488.92)	$\exp(1.92 + 0.79 * b_{706})$ (40.45; 21.72; 27.67)	$\exp(1.82 + 0.66 * b4_{655})$ (40.50; 22.91; 27.67)	$\exp(1.91 + 0.78 * b5_{706})$ (40.45; 21.65; 27.67)
SPOT bands XS3 (cen. 835 nm) and XS1 (cen. 545 nm) (Doxaran et al., 2002)	$\exp(3.01 + 3.13 * XS3_{835} / XS1_{545})$ (27.37; 21.06)	$\exp(2.37 + 3.25 * XS3_{835} / XS1_{545})$ (26.29; 29.62; 16.43)	N/A	$\exp(2.39 + 3.57 * b8_{843} / b3_{561})$ (26.42; 29.79; 16.49)
SPOT bands XS3 (cen. 835 nm) and XS2 (cen. 645 nm) (Doxaran et al., 2002)	$\exp(2.56 + 5.31 * XS3_{835} / XS2_{645})$ (83.15; 50.92)	N/A	N/A	N/A

Table 4
Temporal satellite image coverage from January 2015 to June 2016. Total images from each satellite (Sentinel-2: S-2; Landsat 8: L8) are listed in the table, note that S-2 images first became available July 2015. Satellite acquisitions also depicted in Fig. 4.

Platform	Jan	Feb	Mar	Apr	May	Jun	Jul	Aug	Sep	Oct	Nov	Dec	Jan	Feb	Mar	Apr	May	Jun	Total
L8	1	0	1	2	1	0	0	0	1	1	1	0	1	0	1	1	0	1	12
S-2	–	–	–	–	–	–	1	2	3	1	0	1	1	1	1	0	1	2	24

exposure was found to be highest locally around the five main river mouths (Maistra, Pila, Tolle, Gnocca and Goro), as well as by side channels (Scirocco, Tramontana). Different amounts of river plume exposure were determined for the three arms of the Tolle river mouth, with the highest signal coming from the middle arm and the lowest from the southern arm. Evidence of an extra river mouth with strong outflow between Tramontana and Pila from the remote sensing analysis follows observations made while collecting the field data. The Po della Pila mouth is supposed to transport over 60% of the entire river discharge (Correggiari et al., 2005), but based on the SPM exposure map, this river mouth appears to be on par with the effects from the Po delle Tolle and Busa di Tramontana. A persistent sand bank was observed at the opening of this river mouth, both in the remote sensing images and during sampling in the field. In images taken during high SPM events, it is clear that flow out of Po della Pila is being split into a northern and southern portion after encountering this sand bar. If flow is indeed being slowed out of Po della Pila by the presence of this sand bar, this would provide a mechanism to explain why the flow is high out of the Busa di Tramontana and the unnamed outlet just south of Tramontana. Although this can only be definitively tested with *in situ* hydrodynamic measurements, the potential of using remote sensing SPM images for identifying fine-scale river mouth dynamic patterns is nevertheless well demonstrated here. The time series was able to capture multiple acquisitions of Bora events with low river discharge and one instance with high river discharge. In all events, the river plume is observed to stay closer to the Italian coastline with Bora wind, following results and model predictions made by Falcieri et al. (2014). This is in stark contrast to the situation observed with Scirocco together with high discharge, where the river plume can be observed to extend further east and north (Fig. 6). River plume dynamics during Mistral events appear to be controlled more by river discharge than wind regime. The relationship between wind regime and freshwater outflow on northern Adriatic circulation patterns is complex, but remote sensing images of the river plume can certainly serve as a useful tool for testing hypotheses.

Very low *in situ* water microplastic concentrations were found for the Po di Maistra and delle Tolle mouths, as well as the Busa di Scirocco. Two of these river mouths, namely Maistra and Scirocco, were observed to also have low river plume influence from the remote sensing accumulation map. Maistra is expected to have the smallest outflow of all river mouths (Correggiari et al., 2005), and was thus also found to have the smallest impact from the hydrodynamic accumulation modelling (Fig. 5). The low *in situ* water microplastic concentration measurement from Po delle Tolle is less easily clarified, as this mouth was found to have a substantial influence by both the hydrodynamic and remote sensing accumulation models. There was also a discrepancy between the measured *in situ* concentrations from the middle Tolle mouth and before the Tolle arm divides into three. This suggests that

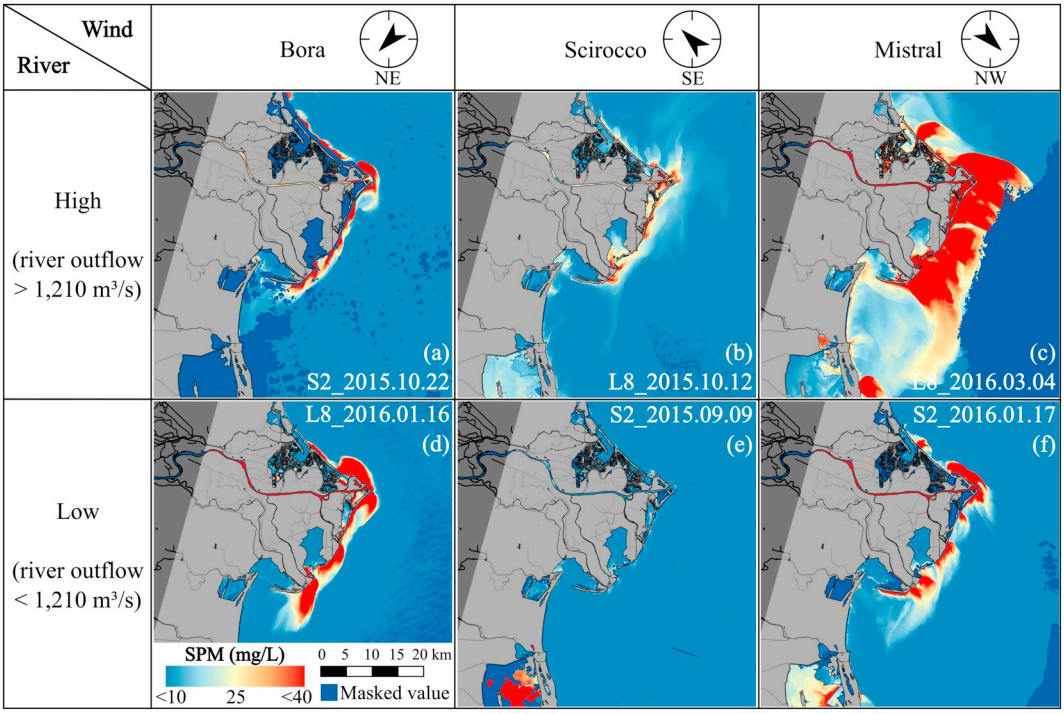

Fig. 6. Combined effect of different wind regimes (Bora, Scirocco or Mistral) with differing river discharge conditions on river plume transportation along the Western Adriatic. River discharge is termed "high" (panels a, b, c) or "low" (panels d, e, f) depending on daily discharge relative to the median (1210 m^3/s) over the entire simulation period. Wind events were classified based on wind direction (indicated by wind compass in each column, pointing in the direction that wind is blowing) and strength (winds in excess of 5 m/s). Suspended Particulate Matter (SPM) values, ranging from low in blue to high in red, depict river plume shape. Masked pixels are depicted in dark blue, land in light gray (outside of area of interest in dark gray). (For interpretation of the references to color in this figure legend, the reader is referred to the web version of this article.)

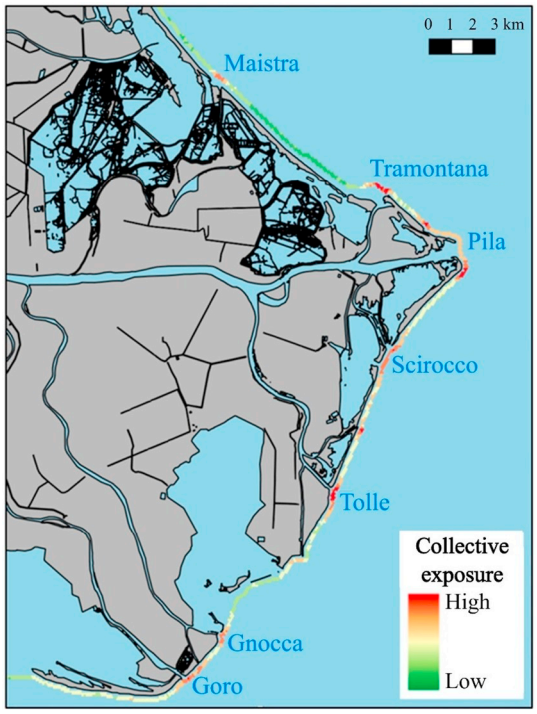

Fig. 7. Composite hexagon (100 m) map of SPM time series, colored by summed daily similarity values to river water. High rates of river plume influence (red) are observed at all five major river mouths and the Busa di Tramontana and di Scirocco, around Po della Pila. Low river plume influence (green) can be observed along the northern coast of the delta. (For interpretation of the references to color in this figure legend, the reader is referred to the web version of this article.)

further accumulation processes may be occurring within the Tolle subarm which have not been captured by the model, and thus warrants further investigation than was feasible within the scope of this study.

3.5. Model validation results

No significant relationship was found when comparing the *in situ* beach sediment microplastic concentrations to the nearest hydrodynamic model grid cell ($p > 0.10$ for Pearson's r and Spearman's ρ). Removal of beach locations that were under more influence from beach tourism and nearby aquaculture (namely Caleri, Levante, Boccasette and Barricata) resulted in a stronger correlation with the hydrodynamic results: Pearson's $r = 0.79$ and Spearman's $\rho = 0.80$ ($p < 0.07$ in both cases). Comparison of *in situ* beach sediment microplastic concentrations with the nearest remote sensing model 30 m hexagon revealed a moderate negative correlation, with Pearson's $r = -0.58$ ($p = 0.05$). No significant correlation was found at the 100 m hexagon resolution. Focusing the comparison to beaches with lesser influence from beach tourism and nearby aquaculture did not reveal an improved correlation. Removal of the styrene-based polymers from the *in situ* beach sediment microplastic concentrations was also considered, given that the majority of the styrene-based polymer group was composed of foamed polystyrene. This particular styrene polymer form is highly buoyant and thus very susceptible to windage during transport as well as potential higher susceptibility for further particle fractionation during beach sediment lab processing. Despite these considerations, removal of this group from *in situ* beach sediment microplastic concentrations was not found to provide any further model improvement.

Comparison between the two models is depicted in Fig. 8, where the normalized remote sensing exposure map is shown next to the hydrodynamic model accumulation map (Fig. 8a). General tendencies for lower normalized values along the coastline north of Pila di Maistra and south of Lido di Volano were similar between the two model results. Strong river mouth signal from Pila, the southern Tolle, Gnocca and Goro were also evident in both maps. Visual dissimilarities were most evident for the river mouths Maistra, Tramontana and Scirocco, where a strong signal was registered by the remote sensing model but not by the hydrodynamic model. In Fig. 8b, the difference of the normalized values (remote sensing normalized values, RS_{norm}, minus hydrodynamic normalized values, HD_{norm}) are displayed as a bar chart aligned along the latitudinal axis. The comparison was made along the full overlap extent of both maps and the distribution is indicated in Fig. 8b with one and two standard deviation gray shaded areas. A slight positive bias is observed, meaning that the RS_{norm} values tend to be higher than the HD_{norm} values, with 95% of all values lying between -0.07 and 0.49. Areas of exceptional variation, indicated by bars lying outside the shaded gray area, were notably the coastline located between Pila and Scirocco and between the northern and central Tolle mouths.

Validation of both accumulation models against all *in situ* measurements did not produce a significant relationship. This is likely due to additional microplastic processes (such as biofouling or sinking) and sources outside of the Po River water which were not included in either model. Artifacts may also have been introduced to the correlation through the *in situ* sediment sampling scheme. In an effort to circumvent potential temporal variability, the extreme high tide line was chosen for the field sampling over the most recent high tide line. Another factor to acknowledge is the assumption of beaching occurring after a particle passes within 250 m of the coastline, representing a substantial simplification of nearshore currents but which was necessary with the given modelling tools. A slightly significant correlation was found between the hydrodynamic accumulation map and *in situ* samples from beaches which were only accessible by boat and not located next to a large harbor. An inverse relationship between amount of beach litter and distance to nearest parking lot has already been established in the Adriatic (Munari et al., 2017), suggesting that beach tourism poses a significant plastic litter source not included in the models. The remote sensing river plume exposure model was not found to have a significant relationship with the *in situ* samples but was very useful in identifying which river mouths were significant outflow contributors during the simulation period. This information can be useful in the set-up of future ocean current models of the Po Delta. A number of factors not incorporated into either the hydrodynamic or the remote sensing model may largely explain the missing correlation. Refuse resulting from the major shipping corridors which cross the Adriatic are posited to account for 20% of all marine plastic litter introduced each year to the sea and the Po River for only 13.5% thereof (Liubartseva et al., 2016). Windage of particles was not accounted for in the hydrodynamic model, which can provide drift speeds up to 25% larger than the current speed (Chubarenko et al., 2016). After particles become beached, wind transportation may move particles laterally or further inland (Munari et al., 2016). Microplastic particle aging within the marine environment was also not represented, including processes of biofouling, further fragmentation, flocculation and aggregation, all which are recognized as important dynamic parameters influencing residence times and transportation pathways (Zhang, 2017). VMP density was simplified to 0.91 g/mL, representative of the average of virgin PE (both high and low density) and PP, which was a necessary assumption given the scope of the study. It would be quite interesting to test how differing particle density for each major plastic type would affect modelled coastal accumulation patterns, especially for the polymer groups most represented in the sediment samples (PE, PP and PS). Seasonality was accounted for in the hydrodynamic model through changing the amount of VMP released dependent upon Po River outflow, but the concentration of microplastic particles was held constant during the entire modelling period. It has been established that river mouth concentrations of microplastic particles can vary by up to three orders of magnitude at different times of the year (Lebreton et al., 2017) and that storm water runoff events can significantly increase river

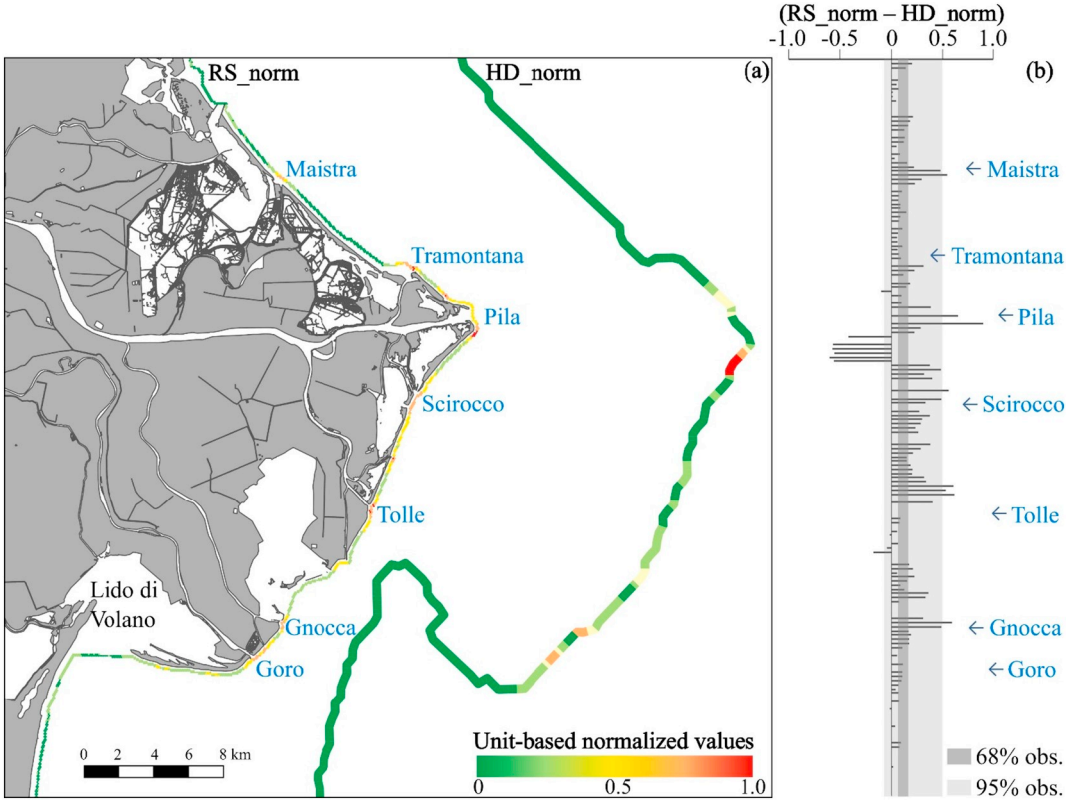

Fig. 8. (a) Remote sensing hexagon-binned (100 m) exposure map (left) next to hydrodynamic model accumulation map (right), both datasets have been unit-based normalized (green low to red high). (b) Difference normalized remote sensing model (RS_{norm}) to normalized hydrodynamic model (HD_{norm}), aligned along the latitudinal axis. Percentage all observations (obs.) at one standard deviation (1-σ, 68%, dark gray) or two (2-σ, 95%, light gray) is indicated, and river mouth position along bar chart is shown in blue italics. (For interpretation of the references to color in this figure legend, the reader is referred to the web version of this article.)

mouth microplastic load (Zhang, 2017). Beaching in this study's hydrodynamic model follows simplifying assumptions made in other studies (Lebreton et al., 2012; Politikos et al., 2017), since the mechanisms controlling onshore-offshore transport of microplastic particles remain unclear (Critchell et al., 2015; Hardesty et al., 2017; Hinata et al., 2017; Moreira et al., 2016). Despite this, these mechanisms likely play a driving role in determining small-scale and temporal variation in sediment microplastic deposition rates (Carlson et al., 2017; Hinata et al., 2017; Schulz et al., 2017; Zhang, 2017).

4. Conclusions and outlook

In situ sampling of both Po River and Adriatic Sea waters revealed microplastic concentrations up to 84 particles/m^3 and beach sediment concentrations up to 78 particles/DW kg. The hydrodynamic modelling approach was able to identify differing beaching rates between various river mouths and suggested that particle beaching mostly occurred within the first 10 days of release. Particles which do not beach within this initial time period (over 80% of all VMP emitted by the Po River) were transported away from the Po Delta coastline. Po River emitted particles that were moved offshore remained offshore, likely due to the continual freshwater input creating water density boundaries that inhibit westward transport. Especially the Po di Goro mouth was identified as effecting higher beaching rates over a much longer stretch of coastline. The suspended sediment remote sensing approach was able to well represent river mouth relative strength, such as the smaller contribution from the southernmost Po delle Tolle river arm or the much larger contribution of Busa di Tramontana in river outflow. Microplastic accumulation exposure maps were constructed from both approaches, which were found to be similar to one another but were not found to have a significant relationship to *in situ* beach sampling. This relationship changed when beaches that were closer to public parking lots and harbors were removed, suggesting that microplastic sources which were not accounted for in either modelling approach are also large contributors to beach microplastic accumulation.

There remain many uncertainties still in our understanding of the transportation and accumulation mechanisms of microplastics (Hardesty et al., 2017) and with this study we offer some insight into these mechanisms within the coastal environment. From the hydrodynamic modelling, we see how particles not beached within the first 10 days are transported away from the coastline. The hydrodynamic model also offers a continual track of VMP transportation and could be used to study VMP distribution in the open sea. The remote sensing model presents snapshots of surface river plume form at a finer spatial resolution over a larger area than computationally feasible with existing ocean current models. River plume exposure during the modelling period could be well captured but this is difficult to translate to actual microplastic accumulation rates. Model assimilation of remote sensing data into ocean current simulation models has begun to gain traction in other oceanographic modelling areas (Miyazawa et al., 2013; Stroud et al., 2009; Zhang et al., 2014), with up to 40% improvements in model forecast root square error. Hardesty et al. (2017) have already suggested the great improvements possible to our understanding of microplastic transportation pathways through integrating simulation model and empirical observations.

Deeper understanding of microplastic sources, pathways and accumulation areas is intrinsic to our ability to mitigate introduction of this pollutant to limnic and marine systems as well as organize clean-up activities. International agreements are already in place forbidding deposition of litter into the Mediterranean marine environment (Mistri et al., 2017; Munari et al., 2016), yet despite these steps this enclosed sea continues to have particularly high concentrations of marine debris

(Cozar et al., 2015; Suaria et al., 2016). Other modelling efforts within the Adriatic suggest that land-based sources of marine litter contribute the majority of marine litter entry into the sea each year (Munari et al., 2017). National borders are not a component of marine plastic debris transportation pathway mechanisms and finding middle ground in national agendas to support concerted legislation efforts are difficult. *In situ* microplastic sampling and sample processing is costly, thus modelling offers a methodology for upscaling point measurements to larger areas than could be feasibly sampled (Hardesty et al., 2017). Freshwater systems, in particular rivers, have been slower to receive the same microplastic research attention as attributed to marine systems (Wagner et al., 2014). Evidence exists that even low-density tourism can still create heavy consumer plastic pollution (Free et al., 2014). Methods for identifying marine debris sources and forecasting accumulation areas have already been put forward as a method to reduce the cost and optimize the effort of remediation activities (Krelling et al., 2017; UNEP, 2016). This study demonstrates the strengths and weaknesses of two separate modelling approaches, providing further tools aiming to answer the suggestion of Hardesty et al. (2017) to develop multipart solutions which can be applied at both local and regional scales to effect change.

Supplementary data to this article can be found online at https://doi.org/10.1016/j.marpolbul.2018.11.045.

Acknowledgements

The authors would like to thank Sandra Lohberger for providing advice and input to both the analysis and writing of the paper. This work was very kindly supported by numerous lab technicians and interns. Sabela Rodríguez Castaño, Sophia Wisböck and Moritz Altenbach in particular provided much appreciated support in image processing. Both Veronika Mitterwallner and Lena Löschel played very important roles in the preparation and analysis of the microplastic samples, and Heghnar Martirosyan and Annika Heymann are thanked for their help with ATR measurements. We would like to extend our thanks to our brave boat captains, Claudio and Sandro, who were willing to take a trio of crazy scientists repeatedly out into the open ocean. This study was partly funded by the German Federal Ministry for Economic Affairs and Energy (Bundesministerium für Wirtschaft und Energie, or BMWi) *via* the DLR Space Administration under the grant numbers 50EE1301 and 50EE1269, and by the Italian National Flagship Program RITMARE of the Italian Ministry of Education, University and Research.

References

Andrady, A.L., 2017. The plastic in microplastics: a review. Mar. Pollut. Bull. 119, 12–22. https://doi.org/10.1016/j.marpolbul.2017.01.082.

Artegiani, A., Paschini, E., Russo, A., Bregant, D., Raicich, F., Pinardi, N., 1997a. The Adriatic Sea general circulation. Part I: Air-sea interactions and water mass structure. J. Phys. Oceanogr. 27, 1492–1514. https://doi.org/10.1175/1520-0485(1997)027<1492:TASGCP>2.0.CO;2.

Artegiani, A., Paschini, E., Russo, A., Bregant, D., Raicich, F., Pinardi, N., 1997b. The Adriatic Sea general circulation. Part II: Baroclinic circulation structure. J. Phys. Oceanogr. 27, 1515–1532. https://doi.org/10.1175/1520-0485(1997)027<1515:TASGCP>2.0.CO;2.

Azzarello, M.Y., van Vleet, E.S., 1987. Marine birds and plastic pollution. Mar. Ecol. Prog. Ser. 37, 295–303. https://doi.org/10.3354/meps037295.

Bignami, F., Sciarra, R., Carniel, S., Santoleri, R., 2007. Variability of Adriatic Sea coastal turbid waters from SeaWiFS imagery. J. Geophys. Res. Oceans 112, C03S10. https://doi.org/10.1029/2006JC003518.

Bolaños, R., Sørensen, J.V.T., Benetazzo, A., Carniel, S., Sclavo, M., 2014. Modelling ocean currents in the northern Adriatic Sea. Cont. Shelf Res. 87, 54–72.

Boldrin, A., Carniel, S., Giani, M., Marini, M., Bernardi Aubry, F., Campanelli, A., Grilli, F., Russo, A., 2009. Effects of bora wind on physical and biogeochemical properties of stratified waters in the northern Adriatic. J. Geophys. Res. Oceans 114, 1492. https://doi.org/10.1029/2008JC004837.

Booij, N., Ris, R.C., Holthuijsen, L.H., 1999. A third-generation wave model for coastal regions: 1. Model description and validation. J. Geophys. Res. Oceans 104, 7649–7666.

Bouwman, H., Evans, S.W., Cole, N., Yive, Nee Sun Choong Kwet, Kylin, H., 2016. The flip-or-flop boutique: marine debris on the shores of St Brandon's rock, an isolated tropical atoll in the Indian Ocean. Mar. Environ. Res. 114, 58–64.

Browne, M.A., Galloway, T.S., Thompson, R.C., 2010. Spatial patterns of plastic debris along estuarine shorelines. Environ. Sci. Technol. 44, 3404–3409. https://doi.org/10.1021/es903784e.

Brunner, K., Kukulka, T., Proskurowski, G., Law, K.L., 2015. Passive buoyant tracers in the ocean surface boundary layer: 2. Observations and simulations of microplastic marine debris. J. Geophys. Res. Oceans 120, 7559–7573. https://doi.org/10.1002/2015JC010840.

Cable, R.N., Beletsky, D., Beletsky, R., Wigginton, K., Locke, B.W., Duhaime, M.B., 2017. Distribution and modeled transport of plastic pollution in the Great Lakes, the world's largest freshwater resource. Front. Environ. Sci. 5 (10377). https://doi.org/10.3389/fenvs.2017.00045.

Campbell, J.W., O'Reilly, J.E., 2005. Metrics for Quantifying the Uncertainty in a Chlorophyll Algorithm: Explicit Equations and Examples Using the OC4.v4 Algorithm and NOMAD data. Ocean Color Bio-optical Algorithm Mini-workshop, Durham, New Hampshire. 27–29 Sept. 2005.

Carlson, D.F., Suaria, G., Aliani, S., Fredj, E., Fortibuoni, T., Griffa, A., Russo, A., Melli, V., 2017. Combining litter observations with a Regional Ocean model to identify sources and sinks of floating debris in a semi-enclosed basin: the Adriatic Sea. Front. Mar. Sci. 4, 1–16. https://doi.org/10.3389/fmars.2017.00078.

Carniel, S., Benetazzo, A., Bonaldo, D., Falcieri, F.M., Miglietta, M.M., Ricchi, A., Sclavo, M., 2016. Scratching beneath the surface while coupling atmosphere, ocean and waves: analysis of a dense water formation event. Ocean Model 101, 101–112. https://doi.org/10.1016/j.ocemod.2016.03.007.

Chubarenko, I., Bagaev, A., Zobkov, M., Esiukova, E., 2016. On some physical and dynamical properties of microplastic particles in marine environment. Mar. Pollut. Bull. 108, 105–112. https://doi.org/10.1016/j.marpolbul.2016.04.048.

Correggiari, A., Cattaneo, A., Trincardi, F., 2005. The modern Po Delta system: lobe switching and asymmetric prodelta growth. Mar. Geol. 222-223, 49–74. https://doi.org/10.1016/j.margeo.2005.06.039.

Cozar, A., Sanz-Martín, M., Martí, E., Ignacio González-Gordillo, J., Ubeda, B., Gálvez, J.Á., Irigoien, X., Duarte, C.M., 2015. Plastic accumulation in the Mediterranean Sea. PLoS One 10, e0121762. https://doi.org/10.1594/PANGAEA.842054.

Critchell, K., Grech, A., Schlaefer, J., Andutta, F.P., Lambrechts, J., Wolanski, E., Hamann, M., 2015. Modelling the fate of marine debris along a complex shoreline: lessons from the Great Barrier Reef. Estuar. Coast. Shelf Sci. 167, 414–426. https://doi.org/10.1016/j.ecss.2015.10.018.

Dekker, A.G., 1993. Detection of Optical Water Quality Parameters for Eutrophic Waters by High Resolution Remote Sensing. Proefschrift Vrije Universiteit Amsterdam, Amsterdam, The Netherlands (237 pp).

van der Wal, M., van der Meulen, M., Tweehuijsen, G., Peterlin, M., Palatinus, A., Viršek, M.K., Coscia, L., Kržan, A., 2015. SFRA0025: Identification and Assessment of Riverine Input of (Marine) Litter. Eunomia Research & Consulting (208 pp).

Doxaran, D., Froidefond, J.-M., Lavender, S., Castaing, P., 2002. Spectral signature of highly turbid waters: application with SPOT data to quantify suspended particulatematter concentrations. Remote Sens. Environ. 81, 149–161.

Dris, R., Imhof, H., Sanchez, W., Gasperi, J., Galgani, F., Tassin, B., Laforsch, C., 2015. Beyond the ocean: contamination of freshwater ecosystems with (micro-)plastic particles. Environ. Chem. 12, 539. https://doi.org/10.1071/EN14172.

Duhec, A.V., Jeanne, R.F., Maximenko, N., Hafner, J., 2015. Composition and potential origin of marine debris stranded in the Western Indian Ocean on remote Alphonse Island, Seychelles. Mar. Pollut. Bull. 96, 76–86. https://doi.org/10.1016/j.marpolbul.2015.05.042.

Falcieri, F.M., Benetazzo, A., Sclavo, M., Russo, A., Carniel, S., 2014. Po River plume pattern variability investigated from model data. Cont. Shelf Res. 87, 84–95. https://doi.org/10.1016/j.csr.2013.11.001.

Fargion, G.S., Mueller, J.L., 2000. Ocean Optics Protocols for Satellite Ocean Color Sensor Validation, Revision 2: Sensor Intercomparison and Merger for Biological and Interdisciplinary Ocean Studies (SIMBIOS) Project Technical Memoranda. NASA/TM-2000-209966/REV2, Rept-2000-04041-0/REV2, NAS 1.15:209966/REV2. NASA, NASA Goddard Space Flight Center, Greenbelt, MD, USA (194 pp). https://ntrs.nasa.gov/search.jsp?R=20000097063.

Free, C.M., Jensen, O.P., Mason, S.A., Eriksen, M., Williamson, N.J., Boldgiv, B., 2014. High-levels of microplastic pollution in a large, remote, mountain lake. Mar. Pollut. Bull. 85, 156–163. https://doi.org/10.1016/j.marpolbul.2014.06.001.

G7 Germany, 2015. Leaders' Declaration G7 Summit, 7–8 June 2015. G7 Germany, Schloss Elmau, Germany (23 pp).

Galgani, F., Hanke, G., Werner, S., Oosterbaan, L., Nilsson, P., Fleet, D., Kinsey, S., Thompson, R.C., van Franeker, J., Vlachogianni, T., Scoullos, M., Veiga, J.M., Palatinus, A., Matiddi, M., Maes, T., Korpinen, S., Budziak, A., Leslie, H., Gago, J., Liebezeit, G., 2013. Guidance on Monitoring of Marine Litter in European Seas: A Guidance Document Within the Common Implementation Strategy for the Marine Strategy Framework Directive. Publications Office of the European Union, Luxembourg.

GESAMP, 2016. Sources, Fate and Effects of Microplastics in the Marine Environment: Part Two of a Global Assessment. Rep. Stud. GESAMP 93. IMO, FAO, UNESCO-IOC, UNIDO, WMO, IAEA, UN, UNEP, UNDP Joint Group of Experts on the Scientific Aspects of Marine Environmental Protection, Rome, Italy (221 pp).

Haidvogel, D.B., Arango, H., Budgell, W.P., Cornuelle, B.D., Curchitser, E., Di Lorenzo, E., Fennel, K., Geyer, W.R., Hermann, A.J., Lanerolle, L., Levin, J., McWilliams, J.C., Miller, A.J., Moore, A.M., Powell, T.M., Shchepetkin, A.F., Sherwood, C.R., Signell, R.P., Warner, J.C., Wilkin, J., 2008. Ocean forecasting in terrain-following coordinates: formulation and skill assessment of the Regional Ocean Modeling System. J. Comput. Phys. 227, 3595–3624.

Hardesty, B.D., Harari, J., Isobe, A., Lebreton, L., Maximenko, N., Potemra, J., van Sebille, E., Vethaak, A.D., Wilcox, C., 2017. Using numerical model simulations to improve the understanding of micro-plastic distribution and pathways in the marine environment. Front. Mar. Sci. 4 (30). https://doi.org/10.3389/fmars.2017.00030.

Heim, B., 2005. Qualitative and Quantitative Analyses of Lake Baikal's Surface-waters Using Ocean Colour Satellite Data (SeaWiFS). Doctoral Thesis. (142 pp).

Hinata, H., Mori, K., Ohno, K., Miyao, Y., Kataoka, T., 2017. An estimation of the average residence times and onshore-offshore diffusivities of beached microplastics based on

the population decay of tagged meso- and macrolitter. Mar. Pollut. Bull. 122, 17–26. https://doi.org/10.1016/j.marpolbul.2017.05.012.
Hoffman, M.J., Hittinger, E., 2017. Inventory and transport of plastic debris in the Laurentian Great Lakes. Mar. Pollut. Bull. 115, 273–281. https://doi.org/10.1016/j.marpolbul.2016.11.061.
Horvat, P., 2015. MICRO 2015 Seminar, Piran, Slovenia. May 2015.
Imhof, H.K., Ivleva, N.P., Schmid, J., Niessner, R., Laforsch, C., 2013. Contamination of beach sediments of a subalpine lake with microplastic particles. Curr. Biol. 23, R867–R868. https://doi.org/10.1016/j.cub.2013.09.001.
Imhof, H.K., Wiesheu, A.C., Anger, P.M., Niessner, R., Ivleva, N.P., Laforsch, C., 2018. Variation in plastic abundance at different lake beach zones - a case study. Sci. Total Environ. 613-614, 530–537. https://doi.org/10.1016/j.scitotenv.2017.08.300.
IOC, SCOR, 1994. Protocols for the Joint Global Ocean Flux Study (JGOFS) Core Measurements. IOC Manuals and Guides 29 (181 pp).
Jambeck, J.R., Geyer, R., Wilcox, C., Siegler, T.R., Perryman, M., Andrady, A., Narayan, R., Law, K.L., 2015. Plastic waste inputs from land into the ocean. Science 347, 768–771. https://doi.org/10.1126/science.1260352.
Jørgensen, P.V., 1999. Standard CZCS Case 1 algorithms in Danish coastal waters. Int. J. Remote Sens. 20, 1289–1301. https://doi.org/10.1080/014311699212731.
Kooi, M., Reisser, J., Slat, B., Ferrari, F.F., Schmid, M.S., Cunsolo, S., Brambini, R., Noble, K., Sirks, L.-A., Linders, T.E.W., Schoeneich-Argent, R.I., Koelmans, A.A., 2016. The effect of particle properties on the depth profile of buoyant plastics in the ocean. Sci. Rep. 6. https://doi.org/10.1038/srep33882.
Krelling, A.P., Souza, M.M., Williams, A.T., Turra, A., 2017. Transboundary movement of marine litter in an estuarine gradient: evaluating sources and sinks using hydrodynamic modelling and ground truthing estimates. Mar. Pollut. Bull. 119, 48–63. https://doi.org/10.1016/j.marpolbul.2017.03.034.
Law, K.L., Thompson, R.C., 2014. Oceans. Microplastics in the seas. Science 345, 144–145. https://doi.org/10.1126/science.1254065.
Lebreton, L.C.-M., Greer, S.D., Borrero, J.C., 2012. Numerical modelling of floating debris in the world's oceans. Mar. Pollut. Bull. 64, 653–661. https://doi.org/10.1016/j.marpolbul.2011.10.027.
Lebreton, L.C.M., van der Zwet, J., Damsteeg, J.-W., Slat, B., Andrady, A., Reisser, J., 2017. River plastic emissions to the world's oceans. Nat. Commun. 8, 15611. https://doi.org/10.1038/ncomms15611.
Lee, J., Hong, S., Song, Y.K., Hong, S.H., Jang, Y.C., Jang, M., Heo, N.W., Han, G.M., Lee, M.J., Kang, D., Shim, W.J., 2013. Relationships among the abundances of plastic debris in different size classes on beaches in South Korea. Mar. Pollut. Bull. 77, 349–354. https://doi.org/10.1016/j.marpolbul.2013.08.013.
Lett, C., Verley, P., Mullon, C., Parada, C., Brochier, T., Pierrick, P., Balnke, B., 2008. A lagrangian tool for modelling ichthyoplankton dynamics. Environ. Model. Softw. 23, 1210–1214.
Lindell, T., Pierson, D., Premazzi, G., Zilioli, E. (Eds.), 1999. Manual for Monitoring European Lakes Using Remote Sensing Techniques. Off. for Off. Publ. of the Europ. Communities, Luxembourg (161 pp).
Liubartseva, S., Coppini, G., Lecci, R., Creti, S., 2016. Regional approach to modeling the transport of floating plastic debris in the Adriatic Sea. Mar. Pollut. Bull. 103, 115–127. https://doi.org/10.1016/j.marpolbul.2015.12.031.
Löder, M.G.J., Gerdts, G., 2015. Methodology used for the detection and identification of microplastics—A critical appraisal. In: Bergmann, M., Gutow, L., Klages, M. (Eds.), Marine Anthropogenic Litter. Springer International Publishing, Cham, pp. 201–227.
Löder, M.G.J., Kuczera, M., Mintenig, S., Lorenz, C., Gerdts, G., 2015. Focal plane array detector-based micro-Fourier-transform infrared imaging for the analysis of microplastics in environmental samples. Environ. Chem. 12, 563. https://doi.org/10.1071/EN14205.
Löder, M.G.J., Imhof, H.K., Ladehoff, M., Löschel, L.A., Lorenz, C., Mintenig, S., Piehl, S., Primpke, S., Schrank, I., Laforsch, C., Gerdts, G., 2017. Enzymatic purification of microplastics in environmental samples. Environ. Sci. Technol. 51, 14283–14292. https://doi.org/10.1021/acs.est.7b03055.
Mani, T., Hauk, A., Walter, U., Burkhardt-Holm, P., 2015. Microplastics profile along the Rhine River. Sci. Rep. 5 (17988). https://doi.org/10.1038/srep17988.
Masura, J., Baker, J., Foster, G., Arthur, C., 2015. Laboratory Methods for the Analysis of Microplastics in the Marine Environment: Recommendations for Quantifying Synthetic Particles in Waters and Sediments Technical Memorandum NOS-OR&R-48. NOAA Marine Debris Program, NOAA Marine Debris Division, Silver Spring, MD, USA (39 pp).
Michaelsen, J., 1987. Cross-validation in statistical climate forecast models. J. Clim. Appl. Meteorol. 26, 1589–1600.
Mistri, M., Infantini, V., Scoponi, M., Granata, T., Moruzzi, L., Massara, F., de Donati, M., Munari, C., 2017. Small plastic debris in sediments from the Central Adriatic Sea: types, occurrence and distribution. Mar. Pollut. Bull. 124, 435–440. https://doi.org/10.1016/j.marpolbul.2017.07.063.
Miyazawa, Y., Murakami, H., Miyama, T., Varlamov, S.M., Guo, X., Waseda, T., Sil, S., 2013. Data assimilation of the high-resolution sea surface temperature obtained from the Aqua-Terra satellites (MODIS-SST) using an ensemble Kalman filter. Remote Sens. 5, 3123–3139. https://doi.org/10.3390/rs5063123.
Mobley, C.D., 1999. Estimation of the remote-sensing reflectance from above-surface measurements. Appl. Opt. 38, 7442. https://doi.org/10.1364/AO.38.007442.
Moreira, F.T., Prantoni, A.L., Martini, B., de Abreu, M.A., Stoiev, S.B., Turra, A., 2016. Small-scale temporal and spatial variability in the abundance of plastic pellets on sandy beaches: methodological considerations for estimating the input of microplastics. Mar. Pollut. Bull. 102, 114–121. https://doi.org/10.1016/j.marpolbul.2015.11.051.
Munari, C., Corbau, C., Simeoni, U., Mistri, M., 2016. Marine litter on Mediterranean shores: analysis of composition, spatial distribution and sources in north-western Adriatic beaches. Waste Manag. 49, 483–490. https://doi.org/10.1016/j.wasman.2015.12.010.
Munari, C., Scoponi, M., Mistri, M., 2017. Plastic debris in the Mediterranean Sea: types, occurrence and distribution along Adriatic shorelines. Waste Manag. 67, 385–391. https://doi.org/10.1016/j.wasman.2017.05.020.
PlasticsEurope, 2014. Plastics – The Facts 2014. An Analysis of European Plastics Production, Demand and Waste Data. PlasticsEurope (33 pp).
PlasticsEurope, 2016. Plastics – THE FACTS 2016. An Analysis of European Plastics Production, Demand and Waste Data. PlasticsEurope (38 pp). http://www.plasticseurope.org/Document/plastics—the-facts-2016-15787.aspx?Page=DOCUMENT&FolID=2.
Politikos, D.V., Ioakeimidis, C., Papatheodorou, G., Tsiaras, K., 2017. Modeling the fate and distribution of floating litter particles in the Aegean Sea (E. Mediterranean). Front. Mar. Sci. 4 (8). https://doi.org/10.3389/fmars.2017.00191.
Poulain, P.-M., 2001. Adriatic Sea surface circulation as derived from drifter data between 1990 and 1999. J. Mar. Syst. 29, 3–32. https://doi.org/10.1016/S0924-7963(01)00007-0.
R Core Team, 2016. R: A Language and Environment for Statistical Computing. R Foundation for Statistical Computing, Vienna, Austria.
Schmidt, L.K., Bochow, M., Imhof, H.K., Oswald, S.E., 2018. Multi-temporal surveys for microplastic particles enabled by a novel and fast application of SWIR imaging spectroscopy - study of an urban watercourse traversing the city of Berlin, Germany. Environ. Pollut. 239, 579–589. https://doi.org/10.1016/j.envpol.2018.03.097.
Schulz, M., van Loon, W., Fleet, D.M., Baggelaar, P., van der Meulen, E., 2017. OSPAR standard method and software for statistical analysis of beach litter data. Mar. Pollut. Bull. 122, 166–175. https://doi.org/10.1016/j.marpolbul.2017.06.045.
Sheavly, S.B., Register, K.M., 2007. Marine debris & plastics: environmental concerns, sources, impacts and solutions. J. Polym. Environ. 15, 301–305. https://doi.org/10.1007/s10924-007-0074-3.
Simeoni, U., Corbau, C., 2009. A review of the Delta Po evolution (Italy) related to climatic changes and human impacts. Geomorphology 107, 64–71. https://doi.org/10.1016/j.geomorph.2008.11.004.
Steppeler, J., Doms, G., Schattler, U., Bitzer, H.W., Gassmann, A., Damrath, U., Gregoric, G., 2003. Meso-gamma scale forecasts using the nonhydrostatic model LM. Meteorog. Atmos. Phys. 82, 75–96.
Stroud, J.R., Lesht, B.M., Schwab, D.J., Beletsky, D., Stein, M.L., 2009. Assimilation of satellite images into a sediment transport model of Lake Michigan. Water Resour. Res. 45 (202). https://doi.org/10.1029/2007WR006747.
Suaria, G., Avio, C.G., Mineo, A., Lattin, G.L., Magaldi, M.G., Belmonte, G., Moore, C.J., Regoli, F., Aliani, S., 2016. The Mediterranean Plastic Soup: synthetic polymers in Mediterranean surface waters. Sci. Rep. 6. https://doi.org/10.1038/srep37551.
Turra, A., Manzano, A.B., Dias, R.J.S., Mahiques, M.M., Barbosa, L., Balthazar-Silva, D., Moreira, F.T., 2014. Three-dimensional distribution of plastic pellets in sandy beaches: shifting paradigms. Sci. Rep. 4 (4435). https://doi.org/10.1038/srep04435.
UNEP, 2016. Marine Plastic Debris and Microplastics – Global Lessons and Research to Inspire Action and Guide Policy Change. United Nations Environment Programme, Nairobi, Kenya (274 pp).
UNESCO, 1994. Protocols for the Joint Global Ocean Flux Study (JGOFS) Core Measurements. UNESCO Publ. No 29. IOC Manuals and Guides, Paris, France. http://unesdoc.unesco.org/images/0009/000997/099739eo.pdf.
Vianello, A., Boldrin, A., Guerriero, P., Moschino, V., Rella, R., Sturaro, A., Da Ros, L., 2013. Microplastic particles in sediments of Lagoon of Venice, Italy: first observations on occurrence, spatial patterns and identification. Estuar. Coast. Shelf Sci. 130, 54–61. https://doi.org/10.1016/j.ecss.2013.03.022.
Vianello, A., Acri, F., Aubry, F.B., Boldrin, A., Camatti, E., Da Rosa, L., Marceta, T., Moschino, V., 2015. Occurrence and Distribution of Floating Microplastics in the North Adriatic Sea: Preliminary Results. MICRO 2015 Seminar, Piran, Slovenia. May 2015.
Wagner, M., Scherer, C., Alvarez-Muñoz, D., Brennholt, N., Bourrain, X., Buchinger, S., Fries, E., Grosbois, C., Klasmeier, J., Marti, T., Rodriguez-Mozaz, S., Urbatzka, R., Vethaak, A.D., Winther-Nielsen, M., Reifferscheid, G., 2014. Microplastics in freshwater ecosystems: what we know and what we need to know. Environ. Sci. Eur. 26 (12). https://doi.org/10.1186/s12302-014-0012-7.
Warner, J.C., Sherwood, C.R., Signell, R.P., Harris, C.K., Arango, H.G., 2008. Development of a three-dimensional, regionl coupled wave, current, and sediment-transport model. Comput. Geosci. 34, 1284–1306.
Warner, J.C., Armstrong, B., He, R., Zambon, J.B., 2010. Development of a coupled ocean–atmosphere–wave–sediment transport (COAWST) modeling system. Ocean Model 35, 230–244.
Zbyszewski, M., Corcoran, P.L., 2011. Distribution and degradation of fresh water plastic particles along the beaches of Lake Huron, Canada. Water Air Soil Pollut. 220, 365–372. https://doi.org/10.1007/s11270-011-0760-6.
Zhang, H., 2017. Transport of microplastics in coastal seas. Estuar. Coast. Shelf Sci. 199, 74–86. https://doi.org/10.1016/j.ecss.2017.09.032.
Zhang, P., Wai, O., Chen, X., Lu, J., Tian, L., 2014. Improving sediment transport prediction by assimilating satellite images in a Tidal Bay model of Hong Kong. Water 6, 642–660. https://doi.org/10.3390/w6030642.
Zhang, W., Zhang, S., Wang, J., Wang, Y., Mu, J., Wang, P., Lin, X., Ma, D., 2017. Microplastic pollution in the surface waters of the Bohai Sea, China. Environ. Pollut. 231, 541–548. https://doi.org/10.1016/j.envpol.2017.08.058.